

Testing gravitational parity violation with coincident gravitational waves and short gamma-ray bursts

Nicolás Yunes,^{1,2} Richard O’Shaughnessy,² Benjamin J. Owen,^{2,3} and Stephon Alexander^{2,4}

¹*Department of Physics, Princeton University, Princeton, NJ 08544, USA.*

²*Department of Physics, Institute for Gravitation and the Cosmos,
The Pennsylvania State University, University Park, PA 16802, USA.*

³*Max Planck Institut für Gravitationsphysik (Albert Einstein Institut), Callinstr. 38, 30167 Hannover, Germany*

⁴*Department of Physics and Astronomy, Haverford College, Haverford, PA 19041, USA.*

Gravitational parity violation is a possibility motivated by particle physics, string theory and loop quantum gravity. One effect of it is amplitude birefringence of gravitational waves, whereby left and right circularly-polarized waves propagate at the same speed but with different amplitude evolution. Here we propose a test of this effect through coincident observations of gravitational waves and short gamma-ray bursts from binary mergers involving neutron stars. Such gravitational waves are highly left or right circularly-polarized due to the geometry of the merger. Using localization information from the gamma-ray burst, ground-based gravitational wave detectors can measure the distance to the source with reasonable accuracy. An electromagnetic determination of the redshift from an afterglow or host galaxy yields an independent measure of this distance. Gravitational parity violation would manifest itself as a discrepancy between these two distance measurements. We exemplify such a test by considering one specific effective theory that leads to such gravitational parity-violation, Chern-Simons gravity. We show that the advanced LIGO-Virgo network and all-sky gamma-ray telescopes can be sensitive to the propagating sector of Chern-Simons gravitational parity violation to a level roughly two orders of magnitude better than current stationary constraints from the LAGEOS satellites.

PACS numbers: 04.30.Nk, 04.50.Kd

I. INTRODUCTION

Several reasons exist to believe that there is some degree of parity violation in gravity, at least at the quantum scale and possibly carrying through to macroscopic scales through the anomaly mechanism. From an experimental standpoint, it is curious that the weak interaction exhibits maximal parity violation, yet the other fundamental forces apparently exhibit none. From a theoretical standpoint, parity violation arises from the standard model of particle physics [1–3], some sectors of string theory [4, 5], and extensions of loop quantum gravity [6–10].

Gravitational parity violation can be encoded in the action as an extension to general relativity (GR) that consists of the addition of an antisymmetric product of curvature tensors coupled to a scalar field, which to leading order in the curvature leads uniquely to Chern-Simons (CS) gravity [11]. Jackiw and Pi [12] demonstrated that the CS term can be covariantly embedded with its three dimensional counterpart as a consistent modification to GR. In the standard model, there exists a radiatively generated one-loop chiral anomaly that gives rise to a CS term coupled to lepton number [13]. In heterotic and Type I superstring theories, the CS term is generated through the Green-Schwarz gauge anomaly-canceling mechanism [14]. In loop quantum gravity, the scalarization of the Barbero-Immirzi parameter coupled to fermions has been shown to lead to an effective CS action [6–10]. Even devoid of a specific fundamental theory, one can also show that the CS term unavoidably arises in effective field theories of inflation as one of the

few non-vanishing, second-order curvature corrections to the Einstein-Hilbert action [15]. Another phenomenological parity-violating extension to GR has been proposed where the fundamental constants of nature (e.g., Newton’s constant) break parity invariance [16].

Most investigations of gravitational wave (GW) signatures of parity violation have focused on *amplitude birefringence*. That is, compared to GR, right circularly-polarized waves are enhanced or suppressed and left circularly-polarized waves are suppressed or enhanced as they propagate [11, 12, 17–19]. Such birefringence occurs when GWs propagate on a flat or curved background. In fact, the propagation of such waves over cosmological distances has been proposed as an explanation of the baryogenesis problem in the early Universe [20] and could have observable effects on the cosmic microwave background [16, 21, 22] and a stochastic GW background [23, 24]. Cosmological GW amplitude birefringence has been discussed in the context of GW observations of cosmological supermassive binary black holes (BHs) with the planned Laser Interferometer Space Antenna (LISA) [18].

Amplitude birefringence arises in propagating modes if the parity operator does not commute with the Hamiltonian. In its most general form, the effect of the plane-wave propagator can be expressed as

$$\begin{pmatrix} h_{+,k}(t) \\ h_{\times,k}(t) \end{pmatrix} = e^{-i\omega t} \begin{pmatrix} u & iv \\ -iv & u \end{pmatrix} \begin{pmatrix} h_{+,k}(0) \\ h_{\times,k}(0) \end{pmatrix}. \quad (1)$$

Here ω is the GW angular frequency, t is some time coordinate, $h_{+,\times,k}$ are the Fourier components of the GW

of wavenumber k , and u and v are multiplicative factors characterizing the translation invariant amplification/suppression of each Fourier mode during propagation in time. The quantity u corrects for background curvature effects: $u = 1$ in a flat-background, but it acquires redshift corrections in a cosmological background (see e.g. [25]). Given a specific modified theory, Eq. (1) can be obtained by solving the modified field equations for the propagating modes of the metric perturbation, where v measures the degree of parity violation. The right- and left-circular polarizations $h_{\text{R,L}} = (h_+ \pm ih_\times)/\sqrt{2}$ then propagate as

$$\begin{pmatrix} h_{\text{R},k}(t) \\ h_{\text{L},k}(t) \end{pmatrix} = e^{-i\omega t} \begin{pmatrix} u+v & 0 \\ 0 & u-v \end{pmatrix} \begin{pmatrix} h_{\text{R},k}(0) \\ h_{\text{L},k}(0) \end{pmatrix}. \quad (2)$$

In the presence of amplitude birefringence, the eigenvalue matrix of the propagator operator remains diagonal, but with modified eigenvalues. Clearly then, right circularly-polarized waves are amplified or suppressed, while left circularly-polarized waves are suppressed or enhanced relative to GR, depending on the sign of v .

The amplitude birefringence discussed above and in the rest of this paper is a pure propagation effect, which accumulates over propagation distance, in contrast with wave generation effects which do not. As the latter cause parity violation “at the source,” their effect is observable at any distance [12, 26]. Wave generation modifications also couple to matter as well as curvature [27], for example leading to weakly composition dependent waveforms in BH-NS versus NS-NS mergers. Recently, [28] studied parity violation in wave generation for extreme-mass ratio inspirals, finding that indeed trajectories and the multipolar generation scheme itself encode such violation at a fundamental level. The influence of such wave generation effects on GW observables would require a full (non-extreme mass ratio) post-Newtonian and multipolar analysis, which is beyond the scope of this paper. Instead, here we concentrate on wave propagation effects only and for simplicity adopt pure GR wave generation without modified-gravity corrections, recognizing that (i) such wave generation effects are calculable on a theory-by-theory basis and (ii) their distance-independent influence on binary phase should be easily distinguishable from any secular amplification accumulated over cosmological distances.

In this paper, we show that an interesting test of gravitational parity violation due to propagation effects can be made with existing instruments: the SWIFT [29] and GLAST/Fermi [30] gamma-ray satellites, and ground-based LIGO [31] and Virgo [32] GW detectors after ongoing upgrades. Such a test relies on the detection of co-incident GW/gamma-ray burst (GRB) events, a possible progenitor of which are neutron star (NS) binary mergers, that lead to a redshift observation either from afterglow or host galaxy identification. The reasons why such events are excellent to constrain parity violation are the same as those outlined in work that proposes the use of GW/GRB events to constrain GRB parameters [33] and

cosmological parameters [25, 34, 35]. Due to the collimation of the jet producing the GRB, the binary’s orbital angular momentum at merger must point along the line of sight to Earth, and thus the GW signal must be highly circularly-polarized. Together with the accurate sky location obtained from the GRB, this allows an accurate distance measurement from the GW signal. This distance measurement can then be compared to the purely electromagnetic distance measurement, which for typical redshifts $z \sim 0.1$ depends only on the Hubble constant. Amplitude birefringence will manifest as a discrepancy between these two distance measurements. If no discrepancy is found, the error on the distance measurements can be used to place upper limits on the possible degree of gravitational parity violation.

The test proposed here is unique in that it employs only the radiative sector of any generic, gravitational parity violating theory. Current constraints on gravitational parity violation concentrate on a specific alternative theory (CS gravity) and explore only its stationary sector through Solar System experiments [36–38] and binary pulsar tests [39]. As such, these tests constrain only specific and local deviations from gravitational parity invariance in the neighborhood of the gravitational source – that is, near Earth in the Solar System case and near J0737-3039 in the binary pulsar case. The test we discuss here constrains *generic parity violation* over distances of hundreds of Mpc, along the light-cone on which the amplitude birefringent GWs propagate.

This test also compares favorably to future GW tests with LISA [18, 19]. The fractional error in a distance measurement is inversely proportional to the signal-to-noise ratio (SNR) ρ . Although the latter is larger in the LISA case, the sensitivity to the parity violating effect is greater here, because this effect also depends on the GW frequency, which is much larger during NS mergers. Propagation effects should accumulate with distance propagated, and on dimensional grounds this distance should be measured in gravitational wavelengths – that is, the effect should be proportional to Df , where D is the distance propagated and f is the GW frequency. While GW/GRB events will have smaller D s and lower ρ s than LISA supermassive BH observations (both by 1–2 orders of magnitude), f is 5–6 orders of magnitude higher for the LIGO-Virgo network. Thus, the sensitivity to parity violation could be 2–3 orders of magnitude better than in the LISA case, although as we shall see later this is somewhat reduced by systematic errors.

The straw-man chosen here to compare against existing tests of gravitational parity violation is CS gravity. In this theory, the magnitude of gravitational parity violation is controlled by a length parameter (in geometric units), proportional to certain time derivatives of the CS coupling field θ . Solar system observations of the LAGEOS satellites [38] have placed the bound $\dot{\theta}_0 < 2000$ km at 2σ when $\dot{\theta}_0 = 0$. (The subscripts refer to evaluation at present, i.e. zero redshift.) We have found that the above constraint can be generalized assuming

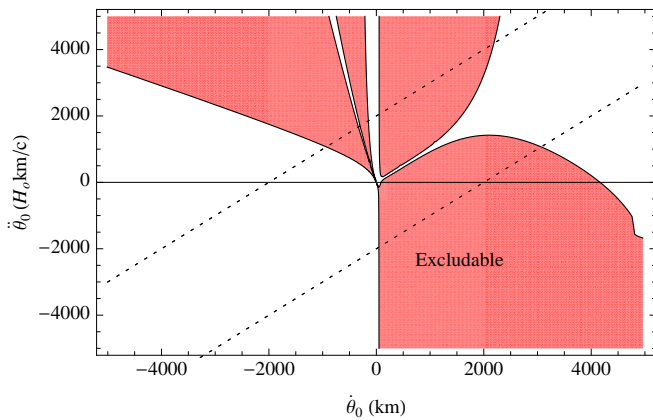


FIG. 1: Given a coincident right-handed GW/GRB detection at an SNR of 10, the gray-shaded region (red in the color version) shows the area of $(\dot{\theta}_0, \ddot{\theta}_0)$ parameter space that could be excluded at 2σ by a measurement of one right-handed short GRB merger waveform consistent with its expected GR amplitude, given host galaxy distance and (measured) chirp mass. The region excluded by Solar System observations ($|\dot{\theta}_0 - \ddot{\theta}_0/H_0| < 2000$ km at 2σ) is outside the dotted lines.

θ evolves on cosmological timescales. Allowing for both $(\dot{\theta}_0, \ddot{\theta}_0)$ to be nonzero to leading order, we can generalize the Solar System constraint via the replacement rule $\dot{\theta}_0 \rightarrow |\dot{\theta}_0 - \ddot{\theta}_0/H_0|$, which then leads to the much more powerful bound $|\dot{\theta}_0 - \ddot{\theta}_0/H_0| < 2000$ km.

Our calculations suggest that the LIGO-Virgo network will be dramatically more sensitive to parity violation, as we show in Fig. 1 for a right-handed GW observation. The gray-shaded regions (red in the color version) show the areas of phase space that could be detected or excluded with a coincident LIGO GW/GRB observation at 2σ . This is to be compared to the regions of phase space ruled out by the generalized Solar System constraints, denoted in the figure as the region outside dotted lines. Inside the dotted lines, the generalized Solar System constraint cannot rule out the CS modification. A GW observation could place much tighter constraints on the allowed region of parity violating phase space. Such constraints are interesting because gravitational parity violation need not be Planck suppressed in the fundamental theory from which CS gravity derives. This is because the effective CS theory is shift-invariant, and thus, the scalar field that sources the correction must be massless, if this symmetry is not to be broken.

A certain asymmetry in the possible constraints we could place on $(\dot{\theta}_0, \ddot{\theta}_0)$ given a single, coincident GW/GRB detection is clearly discernible in Fig. 1. This asymmetry is an artifact of assuming a purely *right-polarized* GW event. In CS gravity, right-polarized signals possess a resonant behavior if $\theta_0 > 0$ for frequencies in the LIGO sensitivity band, which greatly enhances the amount of parity violation and the constraints one could place. This situation, however, reverses if instead we had

assumed a left-polarized GW observation. In such a case, we would have obtained exclusion regions identical to those of Fig. 1 but reflected under $(\dot{\theta}_0, \ddot{\theta}_0) \rightarrow (-\dot{\theta}_0, -\ddot{\theta}_0)$. Therefore, a two-detector observation of a right and a left-polarized GW would allow us to constrain $(\dot{\theta}_0, \ddot{\theta}_0)$ equally well for both positive and negative $\dot{\theta}_0$, thus extending the exclusion regions of Fig. 1.

All the results we just described assume a somewhat idealistic test, where we have ignored certain astrophysical uncertainties, such as inaccuracies in host galaxy identification. Perhaps one of the most important uncertainties relates to the inclination angle. GRB jets are not necessarily perfectly aligned with the line of sight, which implies that the inclination angle is not exactly known *a priori* and the GW signal is not perfectly circularly polarized. Since the inclination angle is degenerate with the luminosity distance in the GW response function, this deteriorates GW measurements of the latter by roughly a factor of two. However, even after taking several such uncertainties into account, we find that $\dot{\theta}_0$ could be constrained at the 10-50 km level, which is still much better than current Solar System constraints and even LISA. Moreover, even when accounting for such uncertainties, coincident GW/GRB measurements could constrain a much larger region of the parity violating phase space all along the light-cone in which GWs propagate.

The remainder of this paper presents additional details that lead to the results described above. We begin with a description of CS gravity and amplitude birefringence in Sec. II as a warm-up for the introduction of generic gravitational parity violation and its GW observable in Sec. III. We then proceed with a somewhat idealized test in Sec. IV, where we compute the modified SNR for a parity-violating signal. Assuming a perfect electromagnetic and GW determination of the luminosity distance, we then compute the constraint one could place on parity violation, assuming the latter can be treated as a linear correction to GR. In CS gravity, however, certain resonances arise in the GW signal at the non-linear level when parity violation is allowed to be strong. Such resonances greatly enhance the parity-violating corrections to the SNR, and thus, allow one to place the much stronger constraints shown in Fig. 1, as we show explicitly in Sec. V. One might worry that resonances could signal the presence of instabilities, but we show that this is not the case in the Appendix. The proposed test, however, is rather idealized because correlations with other parameters and astrophysical uncertainties generically degrade measurements of the luminosity distance. These potential sources of error are discussed in Sec. VI and combined with the idealized analysis to construct realistic estimates of the possible constraints one could place on parity violation.

In the rest of this paper we employ geometric units, where the speed of light and Newton's gravitational constant are set to unity $c = 1 = G$. We further follow the conventions of Misner, Thorne and Wheeler [40], where the metric signature is $(-, +, +, +)$, spacetime indices are denoted with Greek letters, spatial indices with Latin let-

ters and abstract tensors are denoted in boldface type.

II. CHERN-SIMONS MODIFIED GRAVITY

A. CS Basics

CS gravity postulates the addition of a parity-violating term to the vacuum Einstein-Hilbert action (see [11] for a recent review) such that [12]

$$S = \frac{1}{16\pi} \int d^4x \sqrt{-g} \left(R + \frac{1}{4} \theta \mathbf{R}^* \mathbf{R} \right), \quad (3)$$

where g is the determinant of the spacetime metric, R is the Ricci scalar, and

$$\mathbf{R}^* \mathbf{R} = \frac{1}{2} R_{\alpha\beta\gamma\delta} \epsilon^{\alpha\beta\mu\nu} R^{\gamma\delta}_{\mu\nu}, \quad (4)$$

in terms of the Riemann and Levi-Civita tensors \mathbf{R} and ϵ . Such a term is explicitly parity violating because after a spatial triad inversion, the Levi-Civita tensor changes sign, while the square of the Riemann does not. Therefore, the CS correction to the action, the second term in Eq. (3), also changes sign under parity inversion, provided θ is a scalar field, i.e., it is even under parity.

The CS field equations add terms involving $\nabla\theta$ and $\nabla^2\theta$ to the Einstein field equations:

$$\mathbf{G} + \mathbf{C} = 8\pi \mathbf{T}, \quad (5)$$

where \mathbf{G} is the Einstein tensor, \mathbf{T} is the stress energy tensor and \mathbf{C} is the C-tensor

$$C^{\alpha\beta} = (\nabla_\gamma \theta) \epsilon^{\gamma\delta\rho(\alpha} \nabla_\rho R^{\beta)}_{\delta} + (\nabla_\gamma \nabla_\delta \theta) {}^* R^{\delta(\alpha\beta)\gamma}, \quad (6)$$

and parenthesis stand for index symmetrization. The modified field equations are this simple because the CS correction can be thought of as a boundary term that acquires dynamics due to the scalar field coupling [12].

CS gravity can lead to two somewhat distinct theories, depending on whether the CS scalar field is allowed to evolve dynamically or not. In what we shall call “canonical” or “non-dynamical” CS gravity [12] θ is prescribed externally, and a common choice (“static CS gravity”) is to let $\nabla\theta$ be a constant vector pointing in the direction of time defined by cosmic expansion. In what we shall call “dynamical” CS gravity [5, 38, 41] θ is promoted to a dynamical field by adding a kinetic term and a potential $V(\theta)$ to the action, leading to the equation of motion

$$\square\theta + \frac{dV}{d\theta} = -\frac{1}{4} \mathbf{R}^* \mathbf{R}. \quad (7)$$

For the action in Eq. (3) to remain invariant under the shift symmetry $\theta \rightarrow \theta + c$, where c is a constant, the potential must vanish, rendering θ a massless field. In addition to this, the dynamical theory also adds a stress-energy tensor for θ to the right-hand side of Eq. (5).

We consider here both canonical and dynamical CS gravity. In the case of the former, we let θ be an arbitrary function of time, such that it possesses the same symmetries as a Friedman-Roberston-Walker (FRW) spacetime (homogeneity and isotropy). In the case of the latter, the θ field must satisfy its equation of motion, i.e., Eq. (7), whose solution contains a homogeneous and an inhomogeneous piece. The inhomogeneous solution is sourced by $\mathbf{R}^* \mathbf{R}$, which is an extremely small quantity of $\mathcal{O}(h^2)$ [28] in the wave- or radiation-zone (many gravitational wavelengths away from the source), where h is the norm of the metric perturbation. Therefore, the inhomogeneous solution is also small at the location of the observer and, in fact, parity odd because it must possess the same symmetries as $\mathbf{R}^* \mathbf{R}$. Since such a parity odd θ would lead to a parity preserving correction, as then the combination $\theta \mathbf{R}^* \mathbf{R}$ is parity even, we neglect the inhomogeneous solution henceforth. On the other hand, the homogeneous solution forces θ to be a freely propagating wave, but since we require θ to be homogenous and isotropic, so that the background symmetries are satisfied, we shall assume it is a free-function of time only.

At this junction, let us make a brief detour to discuss the units used for the scalar field. As written above, θ has units of squared length, and its time derivative $\dot{\theta}$ defines a length scale (or an inverse energy or mass scale in natural units), which is proportional to the coupling strength of the CS term. To make contact with standard notation [11], θ is here equivalent to $(16\pi G)\theta\alpha^2/\beta$ in the dynamical case or $(16\pi G)\theta\alpha$ in the canonical or non-dynamical case, where (α, β) are CS coupling constants (see eg. [11]).

B. Gravitational Waves in CS gravity

Consider a circularly-polarized, plane GW, propagating on a flat Minkowski spacetime, of the form

$$h_{\text{R,L}}(t, x^i) = h_{0,\text{R,L}} \exp \{ -i [\phi(t) - k_i x^i] \}, \quad (8)$$

where t and x^i are time and space coordinates, k^i is the spatial wave vector and $h_{0,\text{R,L}}$ is some time-independent amplitude. Alternatively, one can work directly with the Fourier transform of the waveform

$$h_{\text{R,L}}(t, x^i) = \frac{1}{(2\pi)^{3/2}} \int dk h_{\text{R,L},k}(t) e^{-ik_i x^i}, \quad (9)$$

where we assume the Fourier modes take the form $h_{\text{R,L},k}(t) = h_{0,\text{R,L}} e^{-i\phi(t)}$.

After linearizing the CS modified field equations and using Eq. (8), the evolution equation for the phase in a right/left circularly-polarized basis becomes

$$i\ddot{\phi} + \dot{\phi}^2 - k^2 = i\lambda_{\text{R,L}} \frac{k \ddot{\theta}}{1 - \lambda_{\text{R,L}} k \dot{\theta}} \dot{\phi}, \quad (10)$$

where overhead dots stand for time derivatives, $k \equiv (k_i k^i)^{1/2}$ is the wave number and where $\lambda_{\text{R}} = +1$ and

$\lambda_L = -1$. Clearly, the phase associated with the right and left polarization obeys different evolution equations. Formally, the phase should also have a subscript $_{R,L}$, but we drop it for now to avoid notational clutter.

Consider now a circularly-polarized, plane GW, propagating on a Friedmann-Robertson-Walker spacetime, of the form

$$h_{R,L}(\eta, \chi^i) = h_{0,R,L} \exp \left\{ -i [\phi(\eta) - \kappa_i \chi^i] \right\}, \quad (11)$$

where η and χ^i are the conformal time and space coordinates, and κ^i is the conformal wave vector. We here let $\phi(\eta)$ be a complex function, such that its imaginary part leads to an amplitude time-dependence. Just as before, we can alternatively work directly with the Fourier transform of the circularly-polarized waveforms

$$h_{R,L}(\eta, \chi^i) = \frac{1}{(2\pi)^{3/2}} \int d\kappa h_{R,L,\kappa}(\eta) e^{-i\kappa_i \chi^i}, \quad (12)$$

where now the Fourier modes take the form $h_{R,L,\kappa}(\eta) = h_{0,R,L} e^{-i\phi(\eta)}$.

Once more, after linearizing the modified field equations in a left/right circularly-polarized basis one finds that the phase obeys a similar equation [18, 21]

$$i\phi'' + (\phi')^2 - \kappa^2 = -2i \frac{\mathcal{H} - \lambda_{R,L} \kappa \theta'' / (2a^2)}{1 - \lambda_{R,L} \kappa \theta' / a^2} \phi' \quad (13)$$

where $\mathcal{H} = a'/a$ is the conformal Hubble parameter, with a the dimensionless scale factor that relates conformal and physical time ($dt = a d\eta$), primes are conformal time derivatives and $\kappa \equiv (\kappa_i \kappa^i)^{1/2}$ is the conformal wave number. One can easily show that Eq. (13) reduces to Eq. (10) in the limit $a(\eta) \rightarrow \text{const.}$

In the flat spacetime case, the modified phase can be obtained by perturbatively solving Eq. (10): expand the phase as

$$\phi = \bar{\phi} + \delta\phi, \quad (14)$$

with $\delta\phi \ll \bar{\phi}$ and assume that $\ddot{\phi} \ll \dot{\phi}^2$ and $\delta\ddot{\phi} \ll \dot{\phi}\delta\dot{\phi}$. The GR solution then returns $\dot{\phi} = \pm k$. For weak CS parity violation ($k\dot{\theta} \ll 1$ and $\ddot{\theta} \ll 1$), the correction to the phase becomes

$$\delta\phi_{\text{FLAT}} = i\lambda_{R,L}\pi f \int_{t_s}^{t_0} \ddot{\theta} dt = i\lambda_{R,L}\pi f (\dot{\theta}_0 - \dot{\theta}_s), \quad (15)$$

where we have defined the GW frequency $f \equiv k/(2\pi)$ and where the subscript “0” and “s” mean the value at the observer and the value at the source respectively. Equation (15) reduces to

$$\delta\phi_{\text{FLAT}} = i\lambda_{R,L}\pi f_0 D \ddot{\theta}_0, \quad (16)$$

if one freezes $\ddot{\theta} = \ddot{\theta}_0 = \text{const.}$, where D is the comoving distance to the source. Notice that it is the combination Df that determines the magnitude of the modification, as already discussed in the Introduction.

In the cosmological case, the CS modification to the phase can be obtained in the same fashion as in the flat case. Expand the phase as in Eq. (14), but now $\bar{\phi}$ and $\delta\phi$ are functions of conformal time and allowed to be complex. Use this phase ansatz to series-expand Eq. (13), assuming that $\delta\phi \ll \bar{\phi}$, $\phi'' \ll (\phi')^2$ and $\delta\phi'' \ll \dot{\phi}'\delta\phi'$, which follows from $\kappa\theta' \ll 1$. The GR solution then returns $\dot{\phi}' = \pm\kappa - i\mathcal{H}$. For weak CS parity violation, the correction to the phase becomes

$$\begin{aligned} \delta\phi_{\text{FRW}} &= i\lambda_{R,L}\pi \int_{t_s}^{t_0} f(t) (\ddot{\theta} - H\dot{\theta}) dt, \\ &= i\lambda_{R,L}\pi a_0 f_0 \left(\frac{\dot{\theta}_0}{a_0} - \frac{\dot{\theta}_s}{a_s} \right), \end{aligned} \quad (17)$$

where we have transformed back to cosmic time using $\theta'' = a^2(\ddot{\theta} + H\dot{\theta})$, with the Hubble parameter $H \equiv \dot{a}/a = a\mathcal{H}$. Notice that the GW frequency is formally time-dependent due to the Hubble dilution, $2\pi f(t) = k - iH(t)$, but the second term is subdominant and can be neglected; cf. Section III and particularly the Appendix [Eq. (A.12)]. Also notice that if $\dot{\theta} = 0$ or $H = 0$, we recover the flat spacetime result in Eq. (16). Simplifying Eq. (17) by Taylor expanding $\dot{\theta} = \dot{\theta}_0 + \ddot{\theta}_0 t$ and using that $a_s \simeq a_0(1 - z)$ we find

$$\delta\phi_{\text{FRW}} \sim -i\lambda_{R,L}\pi f_0 z \left(\dot{\theta}_0 - \frac{\ddot{\theta}_0}{H_0} \right), \quad (18)$$

where $H_0 = (\dot{a}/a)_0$ is the value of the Hubble parameter today and we have assumed a matter-dominated Universe in an $z \ll 1$ expansion, suitable for GW/GRB event. The derivation presented is consistent with the results found in [18], if one expands the latter in the low-redshift limit. This expansion is justified since most LIGO-Virgo GW/GRB events are expected to have $z \ll 1$ [42].

C. Amplitude Birefringence and Parity Violation in CS gravity

The imaginary nature of the CS modification to the phase leads to amplitude birefringence, i.e., the amplitudes of h_L and h_R are modified differently leading to a suppression/enhancement with propagation. For weak parity-violation, $\delta\phi \ll \bar{\phi}$, the exponential suppression/enhancement of the right/left circularly-polarized GW becomes

$$h_{R,L} = \hat{h}_{R,L} e^{-i\delta\phi_{R,L}} \sim \hat{h}_{R,L} (1 - i\delta\phi_{R,L}), \quad (19)$$

where $\hat{h}_{R,L}$ is the GR prediction for the right/left circularly-polarized GW and $\delta\phi_{R,L}$ is given in Eq. (16) or (17). Notice that we have now reinstated the subscript $_{R,L}$ in the phase. Clearly, the parity-violating modification introduces a change in the amplitude since $i\delta\phi_{R,L}$ is a real number. One should note here that the correction

leads to *finite* CS corrections, as $\delta\phi_{\text{R,L}}$ has all along been assumed small. In the Appendix we show that Eq. (19) does not signal the presence of an instability and that indeed the CS correction is formally bounded from above for all relevant values of the CS parameters.

The degree of birefringence can be quantified through v , introduced in Eq. (1). This equation can be rewritten as $h_{\text{R,L}} = \hat{h}_{\text{R,L}}(1 + \lambda_{\text{R,L}}v)$, which can be inverted for v to find

$$v = \frac{1}{2} \left(\frac{h_{\text{R}}}{\hat{h}_{\text{R}}} - \frac{h_{\text{L}}}{\hat{h}_{\text{L}}} \right) = \frac{i}{2} (\delta\phi_{\text{L}} - \delta\phi_{\text{R}}). \quad (20)$$

For weak CS parity violation, we have

$$v_{\text{FLAT,FRW}} = \pi f \delta\dot{\theta}_{\text{FLAT,FRW}}, \quad (21)$$

where we have defined $\delta\dot{\theta}_{\text{FLAT}} = \dot{\theta}_0 - \dot{\theta}_s$ for GWs propagating on flat space and $\delta\dot{\theta}_{\text{FRW}} = \dot{\theta}_0/a_0 - \dot{\theta}_s/a_s$ for GWs propagating on a cosmological background. To measure this effect, it is crucial to know what amplitude the GW signal would have in GR, which is very difficult with ground-based detectors alone, except in the case of binary inspirals associated with GRB.

The analysis presented so far has ignored the pole in the modified dispersion relation of Eqs. (10) and (13) by assuming *weak* CS parity violation. This assumption allows us to expand the pole under $k\dot{\theta} \ll 1$. If this assumption does not hold, then *strong* CS parity violation leads to a resonance in the GW response function that might occur inside the sensitivity band of the GW detector. This resonance enhances the constraints one could place on gravitational parity violation, as we show separately in Sec. V and in the Appendix.

III. GENERIC PARITY VIOLATION IN GW PROPAGATION

Consider a circularly-polarized, plane GW propagating on an FRW background. Let us Fourier decompose this wave as in Eq. (12). In GR, the linearized field equations give the wave equation

$$h''_{\text{R,L},\kappa} + \kappa^2 h_{\text{R,L},\kappa} = -2\mathcal{H} h'_{\text{R,L},\kappa}. \quad (22)$$

The first time derivative of the metric perturbation serves as a dissipative term that controls how the wave amplitude drops adiabatically as the universe expands when \mathcal{H} is non-vanishing.

Parity violation leads to a polarization-dependent modification to the amplitude evolution, and thus, the parity violating generalization of Eq. (22) is the replacement of

$$\mathcal{H} \equiv \frac{a'}{a} \rightarrow \frac{\mathcal{S}'_{\text{R,L}}}{\mathcal{S}_{\text{R,L}}}, \quad (23)$$

where $\mathcal{S}_{\text{R,L}}$ is a polarization-dependent, generalized scale factor. For example, In CS theory, the linearized field

equations reduce to [see e.g., Eq. (18) in [21]]

$$h''_{\text{R,L},\kappa} + \kappa^2 h_{\text{R,L},\kappa} = -2 \left[\frac{\mathcal{H} - \lambda_{\text{R,L}}\kappa\theta''/(2a^2)}{1 - \lambda_{\text{R,L}}\kappa\theta'/a^2} \right] h'_{\text{R,L},\kappa} \quad (24)$$

where we see this is identical to Eq. (22) with the replacement of Eq. (23) and $\mathcal{S}_{\text{R,L}} = a\sqrt{1 - \lambda_{\text{R,L}}\kappa\theta'/a^2}$.

Solutions to the wave equation can be obtained by assuming a GW ansatz of the form $h_{\text{R,L},\kappa}(\eta) = e^{-i\phi(\eta)}$, where ϕ is allowed to be complex. In GR, this reduces Eq. (22) to

$$(\phi')^2 - \kappa^2 = -2i\mathcal{H}\phi', \quad (25)$$

where again we assume $\phi'' \ll (\phi')^2$. For GW wavelengths short compared to the Hubble scale, i.e., $\kappa \gg \mathcal{H}$, the solutions are $\phi' = \pm\kappa - i\mathcal{H}$ to leading order in \mathcal{H}/κ separately for the real and imaginary parts. We are led then to the plane-wave GR solution \hat{h}_{κ}

$$\hat{h}_{\text{R,L},\kappa}(\eta) = \frac{a(\eta_s)}{a(\eta)} e^{\pm i\kappa\eta}, \quad (26)$$

which are the same irrespective of the GW polarity.

The amplitude-birefringent solutions are obtained similarly through Eq. (23). The complex phase then becomes

$$\phi_{\text{R,L}} = \pm\kappa\eta - i \int_{\eta_s}^{\eta} \frac{\mathcal{S}'_{\text{R,L}}}{\mathcal{S}_{\text{R,L}}} d\eta' = \pm\kappa + i \ln \left[\frac{\mathcal{S}_{\text{R,L}}(\eta_s)}{\mathcal{S}_{\text{R,L}}(\eta)} \right]. \quad (27)$$

This results in a plane-wave solution of the form [21]

$$h_{\text{R,L},\kappa}(\eta) = \frac{\mathcal{S}_{\text{R,L}}(\eta_s)}{\mathcal{S}_{\text{R,L}}(\eta)} e^{\pm i\kappa\eta}. \quad (28)$$

This solution is subject to the assumption $\kappa \gg \mathcal{S}'_{\text{R,L}}/\mathcal{S}_{\text{R,L}}$, which is satisfied in CS gravity provided θ' varies on scales much longer than a gravitational wavelength, i.e., $\theta''/\theta' \ll \kappa$. Of course, this assumption does not hold in the immediate neighborhood of the singular point of the wave equation at $\mathcal{S}_{\text{R,L}} = 0$. This singular point is the source of the pole found in the previous section and it is addressed separately in Sec. V and in the Appendix.

We can now explicitly write the propagator in the form of Eq. (1). GW polarizations at conformal time η are given in terms of η_s near the source as in Eq. (1) with the parity violating measure

$$v = \frac{1}{2} \frac{a(\eta)}{a(\eta_s)} \left[\frac{\mathcal{S}_{\text{R}}(\eta_s)}{\mathcal{S}_{\text{R}}(\eta)} - \frac{\mathcal{S}_{\text{L}}(\eta_s)}{\mathcal{S}_{\text{L}}(\eta)} \right]. \quad (29)$$

We note that v reduces exactly to the definition introduced in Eq. (20) when one sets $\mathcal{S}_{\text{R,L}} = a\sqrt{1 - \lambda_{\text{R,L}}\kappa\theta'/a^2}$.

IV. A GW/GRB TEST OF WEAK PARITY VIOLATION

Let us now derive the effect of amplitude birefringence on the GW SNR of a GW/GRB event, as summarized

by [34] and references therein. The single-detector GW power SNR ρ after matched filtering is given by the inner-product

$$\rho^2 = (h|h) \equiv 4 \int_0^\infty df \frac{|\tilde{h}(f)|^2}{S_h(f)}, \quad (30)$$

where S_h is the one-sided power spectral strain noise density of the detector. The quantity $\tilde{h}(f)$ is the Fourier transform of the GW strain measured by a detector, i.e., the response function $h(t)$, which in a parity-preserving theory like GR is given by

$$\hat{h}(t) = F_+ \hat{h}_+(t) + F_\times \hat{h}_\times(t), \quad (31)$$

where $\hat{h}_{+,\times}$ are the GR plus or cross-polarized waveform, while F_+ and F_\times are beam pattern functions that depend on the sky position and a polarization angle ψ (which does not concern us here since we deal with nearly circular polarization). We use overhead hats to remind ourselves that these expressions are valid in GR only. In the Fourier domain, the GW power of a GR signal is approximately

$$|\hat{h}(f)|^2 = F_+^2 |\hat{h}_+|^2 + F_\times^2 |\hat{h}_\times|^2, \quad (32)$$

where $\hat{h}_{+,\times}$ are the Fourier transform of the GR plus or cross-polarized waveform. We have neglected the $F_+ F_\times$ term here, since it vanishes upon integration in the SNR calculation.

For GW signals from binary NS inspirals observed by ground-based detectors, GR predicts that the frequency-domain signal is given to a good approximation by

$$\hat{h}(f) = \hat{\mathcal{A}} f^{-7/6} e^{i\Psi(f)}, \quad (33)$$

where the phase $\Psi(f)$ does not concern us here (except indirectly as it yields precise mass measurements which help determine the distance). We are interested in the amplitude coefficient

$$\hat{\mathcal{A}} = \sqrt{\frac{5}{96\pi^{4/3}}} \frac{\mathcal{M}^{5/6}}{D} \hat{Q}, \quad (34)$$

where \mathcal{M} is the “chirp mass” and D is the distance from source to detector. We neglect corrections to the waveform due to propagation on a cosmological background, as most GW/GRB events will be at low redshift. One can encapsulate the sky position, polarization, and inclination dependence in the factor

$$\hat{Q}^2 = F_+^2 (1 + \xi^2)^2 + 4F_\times^2 \xi^2, \quad (35)$$

where ξ is the cosine of the inclination angle between the orbital angular momentum and the line of sight from source to detector.

A GR binary without orbital precession has a squared SNR of

$$\hat{\rho}^2 = \frac{5}{24\pi^{4/3}} \frac{\mathcal{M}^{5/3}}{D^2} \hat{Q}^2 I_7, \quad (36)$$

and thus an SNR of

$$\begin{aligned} \hat{\rho} \approx & 8.3 \left(\frac{\mathcal{M}}{1.2 M_\odot} \right)^{5/6} \left(\frac{300 \text{ Mpc}}{D} \right) \\ & \times \left(\frac{I_7}{4.7 \times 10^{44} \text{ s}} \right)^{1/2} \left(\frac{F_+^2 + F_\times^2}{2/5} \right)^{1/2}, \end{aligned} \quad (37)$$

where in this last relation we have averaged over angles and assumed an inclination angle such that $\xi^2 = 1$. The noise integrals are defined as

$$I_p = \int_0^\infty df \frac{f^{-p/3}}{S_h(f)}. \quad (38)$$

Note that \hat{Q} , and therefore $\hat{\rho}$, is maximized for $\xi^2 = 1$, i.e., looking down the angular momentum axis.

In the limit of strong signals and weak Gaussian noise, the standard deviation of a single-detector GW amplitude measurement is

$$\frac{\sigma_{\mathcal{A}}}{\mathcal{A}} = \frac{1}{\rho}. \quad (39)$$

With a GW measurement alone it is difficult to convert this into a distance measurement because sky position, ξ and ψ are not easily measured for brief signals such as inspirals. A GW/GRB coincidence provides the needed information. GRBs with observed afterglows have negligible sky position errors. If the GRB jet is tightly collimated, $\xi^2 = 1$ and ψ is irrelevant. In that case, the best-case GW distance measurement error

$$\frac{\sigma_D}{D} = \frac{1}{\rho} \quad (40)$$

is achievable [34]. Recently, [35] pointed out that the above might be an overestimate of the accuracy due to degeneracies between D and ξ^2 . However these degeneracies can be lifted by observing numerous GW/GRB events with a network of non-aligned detectors such as LIGO-Virgo.

The single-detector GW SNR is altered in parity-violating gravity as follows: Combining Eqs. (1) and (31), the strain observed by a detector is seen to be

$$\tilde{h} = F_+ (\hat{h}_+ + i v \hat{h}_\times) + F_\times (\hat{h}_\times - i v \hat{h}_+). \quad (41)$$

and the GW power in the Fourier domain is

$$|\tilde{h}|^2 = |\hat{h}|^2 + 2v (F_+^2 + F_\times^2) \text{Im}(\hat{h}_\times \hat{h}_+^*) + \mathcal{O}(v^2), \quad (42)$$

where again we have neglected the cross terms of the beam pattern functions, as these vanish upon integration. This relation then changes ρ^2 from the GR value $\hat{\rho}^2$ by the replacement

$$\hat{Q}^2 \rightarrow \hat{Q}^2 + 4v (F_+^2 + F_\times^2) \xi (1 + \xi^2) + \mathcal{O}(v^2), \quad (43)$$

in Eq. (36), with \hat{Q}^2 given by Eq. (35).

Assuming that $v \ll 1$, we find that the change in relative SNR due to weak parity violation can be expressed in terms of geometrical factors times a weighted average of the model-dependent factor v :

$$\frac{\rho^2}{\hat{\rho}^2} = 1 + 4 \langle v \rangle \frac{(F_+^2 + F_\times^2) \xi (1 + \xi^2)}{F_+^2 (1 + \xi^2)^2 + 4F_\times^2 \xi^2}, \quad (44)$$

$$\langle v \rangle \equiv \frac{1}{I_7} \int_0^\infty df \frac{v f^{-7/3}}{S_h(f)}. \quad (45)$$

For a perfectly collimated GRB ($\xi^2 = 1$) this reduces to the sky-position-independent first-order result

$$\frac{\rho}{\hat{\rho}} \simeq 1 + \lambda_{\text{R,L}} \langle v \rangle, \quad (46)$$

where the factor of $\lambda_{\text{R,L}}$ arises because $\xi = \pm 1$ depending on the orientation of the face-on source and we have associated a source with $\xi = +1$ with a right-polarized wave. For a weak CS modification to gravity in an FRW background, v reduces to Eq. (21) and the SNR correction reduces to

$$\frac{\rho}{\hat{\rho}} = 1 + \lambda_{\text{R,L}} \pi \delta \dot{\theta}_{\text{FRW}} \frac{I_4}{I_7}, \quad (47)$$

As in Eq. (18), in the limit of slowly-varying $\dot{\theta}$, Eq. (47) reduces to

$$\frac{\rho}{\hat{\rho}} = 1 - \lambda_{\text{R,L}} \pi z \left(\dot{\theta}_0 - \frac{\ddot{\theta}_0}{H_0} \right) \frac{I_4}{I_7}, \quad (48)$$

where we have used that $D \approx z/H_0$ for $z \ll 1$.

In the best case, ρ is a Gaussian with variance unity, and thus a (1σ) -bound on generic parity violation translates into

$$\langle v \rangle < 1/\rho. \quad (49)$$

For weak CS parity violation with $\dot{\theta} = \dot{\theta}_0$, this test would allow one to place the constraint

$$|\dot{\theta}_0| < \frac{1}{\pi} \frac{I_7}{I_4} \frac{1}{z \rho}. \quad (50)$$

With Eq. (36), Eq. (50) can be rewritten in terms of observables as

$$|\dot{\theta}_0^{-1}| > \sqrt{\frac{5}{6}} \pi^{1/3} \sqrt{F_+^2 + F_\times^2} H_0 \mathcal{M}^{5/6} \frac{I_4}{\sqrt{I_7}}. \quad (51)$$

For a double NS GW/GRB, averaging over sky location (such that $F_+^2 = F_\times^2 = 1/5$), $H_0 = 70.5 \text{ km s}^{-1} \text{ Mpc}^{-1}$, and a single interferometer with the present estimate of the “advanced LIGO” fully-commissioned noise performance [43, 44], the threshold is

$$|\dot{\theta}_0| < 1200 \text{ km} \left(\frac{1.2 M_\odot}{\mathcal{M}} \right)^{5/6} \left(\frac{2/5}{F_+^2 + F_\times^2} \right)^{1/2}. \quad (52)$$

Therefore, the 95% confidence threshold for parity violation (compatible with a 2σ constraint) translates into the bound $|\dot{\theta}_0| < 2400 \text{ km}$. Note that the dependences on z and ρ have cancelled out. However, ρ does matter in that z -independent factors which improve ρ , also improve the threshold on $\dot{\theta}_0$, up to a maximum ρ set by systematic errors (see Sec. VI).

V. RESONANT MAGNIFICATION

The analysis presented above neglects a resonance in the parity violating interaction [see e.g., Eqs. (10), (13) or Eq. (29)]. As is apparent from the ubiquitous denominator $1/\mathcal{S}_{\text{R,L}}$ in v , certain wavelengths will be strongly amplified. Such an amplification leads to a *finite* increase in the amplitude correction, as it is shown in the Appendix. Without specifying a functional form for $\mathcal{S}_{\text{R,L}}$, it is nearly impossible to study such resonant behavior, which is why in the rest of this section we assume $\mathcal{S}_{\text{R,L}}$ is given by the CS prediction in Sec. III.

In CS gravity, the resonant frequency f_p and resonant conformal time η_p are such that $\mathcal{S}_{\text{R,L}} = 0$, which reduces to the condition $\kappa_p = \lambda_{\text{R,L}} a_p^2 / \theta_0'$ or in terms of cosmic time

$$f_{p,0} = \frac{\lambda_{\text{R,L}}}{2\pi \dot{\theta}_0}. \quad (53)$$

Nearly the same frequency band will be resonant for *all* GW sources, because the resonance condition depends only on $\dot{\theta}_0$ at the detector.

The estimates of Sec. III for amplification are adequate, provided the GW frequency is sufficiently far from this present-day resonance $f_{p,0}$; the resonant frequency at the source $f_{p,s} = \lambda_{\text{R,L}} / 2\pi \dot{\theta}_s$; and any frequency in between, as these frequencies have generally been resonant in the past. As described in the Appendix, the strongest amplification will occur very close to the present-day resonant frequency $f_{p,0}$, with a bandwidth of $\delta f_p \approx (f_p)^{1/2}$, which reduces to $\delta f_p = [\ddot{\theta} / (2\pi \dot{\theta}^2)]^{1/2}$. Assuming that θ evolves on cosmological scales $\ddot{\theta} = \mathcal{O}(H\dot{\theta})$ implies that $\delta f_p = \mathcal{O}[(H/\dot{\theta})^{1/2}] = \mathcal{O}(10^{-8} \text{ Hz})$.

Similarly, the time period during which the signal is resonant can be computed from the inverse of the resonance bandwidth, or equivalently from the rate of change of the resonant conformal time η_p with respect to conformal wavenumber κ : $\mathcal{R} \equiv d\eta_p / d\kappa_p$. Let us define the squared amplitude $\mathcal{F}_{\text{R,L}} \equiv \mathcal{S}_{\text{R,L}}^2$, which is a function of two independent variables: η_p and κ_p . Requiring that $d\mathcal{F}_{\text{R,L}} = 0$ leads to

$$\frac{d\eta_p}{d\kappa_p} = - \frac{d\mathcal{F}_{\text{R,L}}/d\kappa_p}{d\mathcal{F}_{\text{R,L}}/d\eta_p}, \quad (54)$$

and rewriting this equation slightly we find

$$\mathcal{R} = - \frac{d}{d\kappa} \left(\frac{\mathcal{F}_{\text{R,L}}}{\mathcal{F}'_{\text{R,L}}} \right), \quad (55)$$

where we have used the fact that $\mathcal{F}_{R,L} = 0$ at resonance.

Although the resonance bandwidth is small, if a resonance is present in the sensitive band of the GW detector it will greatly enhance the constraints of the previous section. In what follows, we compute the enhancement of the simple GW/GRB test discussed in Sec. IV if the resonance is in-band. We begin by assuming that the GW signal detected is parity violating and one searches over the data with parity-violating templates. Such considerations lead to an optimal constraint related to the intrinsic SNR of the parity-violating templates. We follow this analysis by considering a parity-violating signal that is filtered with a GR template. By doing so, one incurs a fundamental error in the determination of parameters induced by the assumption that the data contains a GR template (see e.g., [45] for a more detailed discussion of fundamental bias in GW astrophysics).

A. Optimal Strategy

1. Signal-to-Noise Ratio and an Optimal Test

The presence of a resonance in the frequency band where searches are performed leads to an amplification of parity violation. Such an amplification can lead to a stronger constraint than the one we considered in Sec. IV. Of course, the constraint is largest when the search is performed with templates that account for such parity violation. We consider such cases in this subsection.

Let us then assume that some of the detected frequencies are resonant and that one correctly identifies all signal power associated with the event to the correct parity-violating template. The SNR then becomes¹

$$\begin{aligned} \rho^2 &\equiv 4 \int_0^\infty df \frac{|\tilde{h}|^2}{S_h(f)} = 4 \int_0^\infty \frac{df}{S_h} \left| \tilde{h}_R F_R + \tilde{h}_L F_L \right|^2 \quad (56) \\ &= \int_0^\infty \frac{df}{S_h} \left\{ (X_R^2 + X_L^2) \left(|\hat{h}_+|^2 + |\hat{h}_\times|^2 \right) (F_+^2 + F_\times^2) \right. \\ &\quad + 2 (X_R^2 - X_L^2) (F_+^2 + F_\times^2) \text{Im} \left(\hat{h}_\times \hat{h}_+^* \right) \\ &\quad \left. + 2 X_R X_L \left(|\hat{h}_+|^2 - |\hat{h}_\times|^2 \right) (F_+^2 - F_\times^2) \right\}, \quad (57) \end{aligned}$$

where we have defined $F_{R,L} \equiv (F_+ + \lambda_{R,L} F_\times)/\sqrt{2}$ and $X_{R,L} \equiv (\mathcal{F}_{R,L,s}/\mathcal{F}_{R,L,0})^{1/2}$, and where we have assumed h_+ and h_\times are uncorrelated, so that their integrated product vanishes. Recall that hatted quantities correspond to the GR expectation, so that $\hat{h}_{+,\times}$ are the Fourier transform of the GR, plus or cross-polarized

waveform. Notice that this expression reduces to the GR result when $X_R = X_L = 1$ and to the expression in Eq. (44) in the linear approximation $X_{R,L} \sim 1 + \lambda_{R,L} v$.

The above expression can be simplified somewhat if we assume the source is at $\xi = \pm 1$. We then find

$$\begin{aligned} \rho^2 &= \frac{5}{12\pi^{4/3}} \frac{\mathcal{M}^{5/3}}{D^2} (F_+^2 + F_\times^2) \\ &\times \int_0^\infty \frac{df}{S_h} f^{-7/3} [(X_R^2 + X_L^2) \pm (X_R^2 - X_L^2)] . \quad (58) \end{aligned}$$

The beam-pattern functions then only modify the overall coefficient of the SNR, and thus we can rewrite the SNR in the more familiar form

$$\rho^2 = 2\mathcal{A}^2 \int_0^\infty \frac{df}{S_h} f^{-7/3} [(X_R^2 + X_L^2) \pm (X_R^2 - X_L^2)] , \quad (59)$$

Given a single detector, we cannot distinguish between a purely right, or purely left-polarized signal, so effectively we measure either ρ_R or ρ_L , where we have defined

$$\rho_{R,L}^2 = 4 \frac{\mathcal{A}^2}{1+z} \int_0^\infty df \frac{f^{-7/3}}{S_h(f)} (1+z) \left| \frac{\mathcal{F}_{R,L}(\eta_s, k)}{\mathcal{F}_{R,L}(\eta_0, k)} \right| \equiv \hat{\rho}^2 \mathcal{G}_{R,L}^2 , \quad (60)$$

and the amplification factor is

$$\mathcal{G}_{R,L}^2 \equiv \frac{1}{I_7} \int_0^\infty df \frac{f^{-7/3}}{S_h(f)} (1+z) \left| \frac{\mathcal{F}_{R,L}(\eta_s, k)}{\mathcal{F}_{R,L}(\eta_0, k)} \right| . \quad (61)$$

We have here used that $\hat{\rho} = 4\mathcal{A}^2 I_7 / (1+z)$ as shown in Eq. (36), but we have included a factor of $(1+z)^{-1}$ to map between comoving and luminosity distances. This result generalizes the linear, weak-amplification expression of Eq. (48).

Let us now show that the above reduces to the results of Sec. IV in the weak parity violation limit. Assuming the resonant frequencies are very large (i.e., $k_0 \dot{\theta} \ll 1$) and that the source is at low redshift $DH_0 \ll 1$, the resonant factor becomes to leading order

$$\left| \frac{\mathcal{F}_{R,L}(\eta_s, k)}{\mathcal{F}_{R,L}(\eta_0, k)} \right| \simeq 1 - 2\pi f D \lambda_{R,L} \left(\dot{\theta}_0 H_0 - \ddot{\theta}_0 \right) . \quad (62)$$

We recognize the right-hand side as simply $1 + 2\lambda_{R,L} v$ and inserting this back into the SNR we find

$$\begin{aligned} \rho^2 &\simeq \hat{\rho}^2 \frac{1}{I_7} \int_0^\infty df \frac{f^{-7/3}}{S_h(f)} (1 + 2\lambda_{R,L} v) , \\ &\simeq \hat{\rho}^2 \left(\frac{1}{I_7} \int_0^\infty df \frac{f^{-7/3}}{S_h(f)} + 2\lambda_{R,L} \frac{1}{I_7} \int_0^\infty df \frac{f^{-7/3}}{S_h(f)} v \right) , \\ &\simeq \hat{\rho}^2 (1 + 2\lambda_{R,L} \langle v \rangle) , \quad (63) \end{aligned}$$

where $\langle v \rangle$ was defined in Eq. (45). Notice that this expression reduces to Eq. (46), upon linearizing the square-root.

A test of parity violation then presents itself. Let us assume that a GW detection has been made coincident with

¹ Technically, the one-sided SNR integral arises from a more general, two-sided overlap integral [46], acting on a real-valued (i.e., single polarization) strain signal $h_+(t)$. Even though the $\mathcal{F}_{R,L}$ is not symmetric in f , the Fourier transform can be folded together using that $\mathcal{F}_R(f) = \mathcal{F}_L(-f)$.

a GRB event at a known distance, so that the chirp mass and $\hat{\rho}$ (the GR expectation) are unambiguously known. Then, parity violation can be distinguished from a (2σ) -statistical fluctuation if $|\rho_{\text{R,L}}/\hat{\rho} - 1| > 2/\hat{\rho}$ [cf. Eq. (50)]. If such a violation is not observed, one can rule out points in the $(\dot{\theta}, \ddot{\theta})$ space. In particular, $(\dot{\theta}_0, \ddot{\theta}_0)$ values that lead to

$$|\mathcal{G}_{\text{R,L}} - 1| > \frac{2}{\hat{\rho}}, \quad (64)$$

can be excluded; inversely, $(\dot{\theta}_0, \ddot{\theta}_0)$ values that lead to the opposite relation cannot be distinguished from pure GR with a single observation.

2. Numerical Implementation

The implementation of the test in Eq. (64) requires the calculation of the amplitude enhancement factor $\mathcal{G}_{\text{R,L}}$, which in turn requires knowledge of the ratio of $\mathcal{F}_{\text{R,L}}$ at the source and at the observer location. The latter can be rewritten as

$$(1+z) \left| \frac{\mathcal{F}_{\text{R,L}}(\eta_s, k)}{\mathcal{F}_{\text{R,L}}(\eta_0, k)} \right| = \left| \frac{1 - f/(a_s f_{p,s})}{1 - f/(a_0 f_{p,0})} \right|, \quad (65)$$

where $a_0/a_s = 1+z$ and we have defined the resonant frequencies at the source $f_{p,s}$ and at the observer $f_{p,0}$. The resonant or pole frequency at the observer is simply $f_{p,0} = \lambda_{\text{R,L}}/(2\pi\theta_{p,0})$, while that at the source can be approximated as

$$f_{p,s} = f_{p,0} + \frac{df}{dt}\delta t = f_{p,0} - \frac{D}{2\pi\mathcal{R}} + f_{p,0}H_0D, \quad (66)$$

where we have used that $f = \kappa/(2\pi a)$, $\dot{f}_p = \kappa'_p/(2\pi a^2) - \kappa_p\mathcal{H}/(2\pi a^2)$, $\kappa'_p = \mathcal{R}^{-1}$ and $\delta t = -D$. Combining $f_{p,s}$ with the appropriate redshift factors that arise in $a_s \approx (1-z)a_0$, we find

$$a_s f_{p,s} \approx f_{p,0} - \frac{D}{2\pi\mathcal{R}} + \mathcal{O}(k_{p,0}^2 H_0^2), \quad (67)$$

where the last term of Eq. (67) has cancelled.

The calculation of the enhancement factor then requires knowledge of \mathcal{R} , which following Eq. (55) reduces to

$$\mathcal{R} = \frac{\lambda_{\text{R,L}}}{4H_0} \left(\dot{\theta}_0 - \frac{\ddot{\theta}_0}{H_0} \right) \left[1 - \frac{\lambda_{\text{R,L}} k_{p,0}}{2} \left(\dot{\theta}_0 + \frac{\ddot{\theta}_0}{H_0} \right) \right]^{-2}. \quad (68)$$

Using further the fact that $k_{p,0} = f_{p,0}/(2\pi) = \lambda_{\text{R,L}}/(4\pi^2\dot{\theta}_0)$, we can simplify the above expression to

$$\mathcal{R} = \frac{1}{2\pi f_{p,0} H_0 (1-q)}, \quad (69)$$

$$q \equiv \ddot{\theta}_0/(\dot{\theta}_0 H_0), \quad (70)$$

where the dimensionless parameter q is $\mathcal{O}(1)$ for slowly-varying $\dot{\theta}$. Using this expression and in the limit $z \approx H_0 D \ll 1$, Eq. (67) reduces to the extremely simple relation

$$a_s f_{p,s} \approx f_{p,0} [1 + z(1-q)]. \quad (71)$$

In the local universe or for slowly-varying $\dot{\theta}$, the present-day and source-frame resonant frequencies are nearly identical. More precisely, the first-order approximation used in Eq. (67) to relate these frequencies implicitly requires $z|(1-q)| \ll 1$, or

$$z|\ddot{\theta}_0 - H_0\dot{\theta}_0| \ll |H_0\dot{\theta}_0|, \quad (72)$$

corresponding to the requirement that $\delta\dot{\theta}_{\text{FRW}}$ be small. The analysis presented here does not formally apply when the pole frequency is rapidly varying, i.e., when Eq. (72) is violated. However, even then, non-resonant and resonant amplification will generically occur and one should still be able to constrain gravitational parity violation. The results we present below, however, are not valid in this region.

The integrals in Eq. (60) and (61) are evaluated with the estimated NS-NS optimized spectral noise density of [43] and numerically converting them into Riemann sums and the Fourier integrals into Fourier series. In doing so, we must choose a frequency discretization df , which is related to the observation time T via $df \simeq 1/T$. Full coherent recovery of the amplified waveform clearly corresponds to an unrealistically long coherently-integrated data stream: for a $T = 1$ year long integration, $df = \mathcal{O}(1/\text{yr}) \simeq 10^{-8} \text{ Hz}$. In practice, due to detector dropouts and nonstationarity of the noise, the longest integration times are 2048 s [47], imposing a minimum frequency discretization of $df \simeq 1/T \simeq 5 \times 10^{-4} \text{ Hz}$. A search strategy based on these limited data intervals will always recover a somewhat smaller resonant contribution to the total SNR than if one were to integrate for larger T , which then implies less limiting constraints on $(\dot{\theta}_0, \ddot{\theta}_0)$, assuming the same SNR threshold. However the dependence on df is generally quite weak. We have verified these statements by numerically computing the integrals in Eq. (60) and (61) both with $df = 10^{-8} \text{ Hz}$ and $df = 1/2048 \text{ Hz}$ and checking that the changes to Fig. 2 (described below) are hardly visible. In what follows, we shall adopt a realistic frequency resolution of $df = 1/2048 \text{ Hz}$.

The integration of the resonant amplitudes are also formally ill-defined when the integrand sweeps through the resonance $f \rightarrow f_{p,0}$, as then $\mathcal{F}_{\text{R,L}}(\eta_0, k)$ vanishes. Such divergent behavior can be cured by regularizing all integrals, i.e., by cutting out a region of size ϵ about the resonant frequency at present ($f_{p,0}$). Such a regularization is valid because the SNR depends logarithmically on the regulator, as we show explicitly in the Appendix. We choose here $\epsilon = \delta f_p$, but we have checked that choosing $\epsilon = df = 10^{-4} \text{ Hz}$, for example, does not visually affect any of the plots. This regularization is allowed

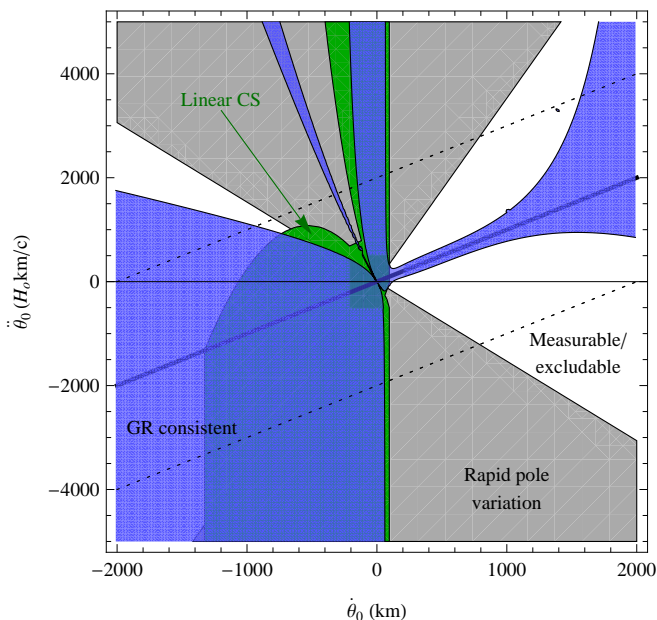


FIG. 2: The blue shaded region corresponds to values of $(\dot{\theta}_0, \ddot{\theta}_0)$ for which parity violation is too small to be measured with a coincident GRB/GW event. The region outside this blue-shaded area can be measured or excluded given a single, GW/GRB event at $\hat{\rho} = 10$. The boundaries of the blue-shaded region correspond to the best $(\dot{\theta}_0, \ddot{\theta}_0)$ constraints one could place. The thick solid line corresponds to the values of $(\dot{\theta}_0, \ddot{\theta}_0)$ for which there is no parity violation ($\mathcal{G}_R = 1$), and thus it represents an absolute theoretical limit to the constraints one could place on CS amplitude birefringence. The dotted lines bracket the values of $(\dot{\theta}_0, \ddot{\theta}_0)$ that are allowed by Solar System constraints. Consequently, the regions outside the dotted lines (not shaded in the figure) have already been excluded by Solar System tests. The green-shaded region shows where the linear, weak-parity approximation of Sec. IV is valid, while the gray-shaded region shows where the linear cosmological expansion of Eq. (67) breaks down. Our calculations suggest that LIGO/Virgo will be able to see or rule out the entire area outside the blue-shaded region, excluding a much larger region of parameter space than Solar System constraints.

within the context of linear propagation theory because the resonant amplification enhances the waveform only to $h f / \delta f_p \ll 1$. Even though the enhancement factor is formally large, $f / \delta f_p \simeq O(10^{10})$, the overall correction is clearly small as typical GW strains are $h = O(10^{-22})$. In the Appendix, we show in more detail that regularizing these integrals induces a negligible error in the SNR.

3. Results and Discussion

Figure 2 shows numerical results for the implementation of the test devised in Eq. (64). The blue-shaded region, labeled *GR consistent*, corresponds to values of $(\dot{\theta}_0, \ddot{\theta}_0)$ for which we cannot distinguish between GR and

CS gravity, i.e., values for which $|\mathcal{G}_R - 1| < 2/\hat{\rho} = 2/10$. This region is generated assuming $D = 600$ Mpc and $\hat{\rho} = 10$ as a fiducial threshold, which could occur in advanced LIGO given a NS-NS merger at an optimal sky location. Given a coincident GRB/GW detection that is non-parity violating, LIGO/Virgo will be able to observe or rule out the area *outside* the blue-shaded region in the figure, which is why we have labeled it *measurable/excludable*. Observe that the blue-shaded region in this figure corresponds to the non-shaded region in Fig. 1.

The boundary of the blue-shaded region in Fig. 2 denotes the best bound that one could place on $(\dot{\theta}_0, \ddot{\theta}_0)$ given a coincident GRB/GW detection consistent with general relativity. This boundary corresponds to values of $(\dot{\theta}_0, \ddot{\theta}_0)$ for which $|\mathcal{G}_R - 1| = 2/\hat{\rho} = 2/10$. The Solar System constraint $\dot{\theta}_0 < 2000$ km with $\ddot{\theta}_0 = 0$ is outside the plotting range of this figure. One can generalize or improve on the Solar System constraint via the map $|\dot{\theta}_0| \rightarrow |\dot{\theta}_0 - \ddot{\theta}_0/H_0|$, assuming the entire right-hand side can be treated as a constant, evolving on timescales much larger than the orbital velocity of the LAGEOS satellites. Doing so, the improved Solar system constraint becomes $|\dot{\theta}_0 - \ddot{\theta}_0/H_0| < 2000$ km. We have plotted this constraint with two diagonal dotted lines in Fig. 2. The region between these dotted lines is consistent with GR and cannot be ruled out, while the area outside of the dotted lines can be excluded with the improved Solar System constraint.

We can now compare this generalized Solar System constraint (the dotted lines) to the possible GW/GRB constraints (the boundary of the blue-shaded region). Figure 2 shows that the latter largely is inside the former when $\dot{\theta}_0 > 0$, which implies GW/GRB constraints would be better than the generalized Solar System constraints. When $\dot{\theta}_0 < 0$ the GW/GRB constraint is not as good with a single detector, as CS parity violation would then be non-resonant in \mathcal{G}_R . Such an issue is circumvented if either (a) two GW detectors are used to extract both h_R and h_L for a non-optimally aligned source $|\xi| \neq 1$ (we discuss this in the next paragraph) or (b) two sources, one right- and one left-handed, have been observed. Furthermore, if we assume $\ddot{\theta}_0 = 0$ as in the standard Solar System constraint, or more generally whenever $|\ddot{\theta}_0| < 100 H_0 \text{ km s}^{-1}$, our results suggest that a GW/GRB detection could constrain $\dot{\theta}_0 < 100$ km. This bound is 20 times stronger than the current Solar System constraint ($\dot{\theta}_0 < 2000$ km). Such enhancements in the GW constraints relative to those presented in Sec. IV are clearly due to the CS resonance in the SNR.

Resonance amplification for a right-circularly polarized GW only occurs when the integrand of the amplitude factor \mathcal{G}_R contains a pole, which leads to the logarithmic divergence discussed in the Appendix. For $\theta_0 < 0$, the amplification of right-handed signals is suppressed as the pole moves to negative frequencies; constraints from right-handed measurements on $\dot{\theta}_o, \ddot{\theta}_o$ are therefore not as strong. The situation reverses, however, if the GW is left-polarized, as then the \mathcal{G}_L regions are identical to the \mathcal{G}_R

ones in Fig. 2 but with $(\dot{\theta}_0, \ddot{\theta}_0) \rightarrow (-\dot{\theta}_0, -\ddot{\theta}_0)$. Therefore, the two-detector detection of a right and a left-polarized GW would allow us to constrain $(\dot{\theta}_0, \ddot{\theta}_0)$ equally well for both positive and negative $\dot{\theta}_0$. More precisely, with such a detection one would be able to constrain $|\dot{\theta}_0| < 100 \text{ km}$ for any $|\ddot{\theta}_0| < 100 H_0 \text{ km s}^{-1}$.

An interesting feature of CS parity violation not appreciated with Solar System constraints is that for certain values of $(\dot{\theta}_0, \ddot{\theta}_0)$ amplitude birefringence can actually vanish. In some sense, for these values of the derivatives of the CS coupling, the CS correction conspires with the cosmological expansion to lead to no parity violation. Such values of $(\dot{\theta}_0, \ddot{\theta}_0)$ then constitute the ultimate theoretical limit to which CS gravity can be constrained. These values of the derivatives of the CS coupling are such that $\mathcal{G}_{\text{R,L}} = 1$, which implies $\rho = \hat{\rho}$. This degeneracy occurs when $f_{p,0} = f_{p,s}$ or simply when $\ddot{\theta}_0 = H_0 \dot{\theta}_0$, which is simply a straight line in the $(\dot{\theta}_0, \ddot{\theta}_0)$ phase space. We have plotted this linear relationship as a solid diagonal line in Fig. 2. Observe that this line is always inside the blue-shaded region, as it should, as the latter represents precisely the region where a GW/GRB measurement does not have the sufficient accuracy to see parity violation given an SNR of 10.

Although resonant amplification generally occurs for any prescribed form for θ , the Taylor expansion used in Eq. (66) to relate source quantities to observer quantities breaks down for certain values of $(\dot{\theta}_0, \ddot{\theta}_0)$. More precisely, when $(\dot{\theta}_0, \ddot{\theta}_0)$ is such that $|z(1-q)| = \mathcal{O}(1)$ or equivalently $|H_0 \dot{\theta}_0 - \ddot{\theta}_0| = \mathcal{O}(H_0 \dot{\theta}_0/z)$, the pole frequency changes rapidly and the Taylor expansion of Eq. (66) is not valid. One might then worry that our analysis breaks down in this region and the bounds quoted earlier in terms of the boundary of the blue-shaded region would not be valid, as higher-order terms in Eq. (66) would be needed. To get a sense of the $(\dot{\theta}_0, \ddot{\theta}_0)$ values for which this happens, in Fig. 2 we have shaded in gray the region where $|z(1-q)| > 0.5$ and labeled it *rapid pole variation*. Observe that this region does not overlap the blue-shaded region for $\dot{\theta} > 0$, which explicitly shows that the bounds proposed above still hold. Of course, one can shrink this gray region by Taylor expanding Eq. (66) to second-order if needed, at the expense of introducing a new parameter $\ddot{\theta}_0$.

The numerical results we have presented here do recover the linear approximation [i.e., Eqs. (48) and (18)] for the $(\dot{\theta}_0, \ddot{\theta}_0)$ values where this approximation is valid, i.e., where there is no resonance in the detection band. The source and observer resonances are out of band provided either $f_{p,0} < -\langle f \rangle$ and $f_{p,0} > 300\text{Hz}$ (for the suppressed frequency being negative or out of the most sensitive band) or $f_{p,s} > 500\text{Hz}$ and $f_{p,s} < -\langle f \rangle$ (when the resonance is well out of band or negative). In order to visualize this in the context of the bounds placed by the boundary of the blue-shaded region in Fig. 2, we have shaded in green the linear approximation region and labeled it *linear CS*. Observe that the linear approximation breaks down for all physically interesting and accessible

$\dot{\theta}_0 > 0$: a resonance generically appears inside the LIGO band. Notice that this is not the case for LISA, as this instrument is sensitive to much lower frequency GWs, for which the resonance is always out of band if one saturates $\dot{\theta}_0$ with the Solar system constraint.

Finally, we have checked that the constraints presented here are formally independent of distance to the source for $(\dot{\theta}_0, \ddot{\theta}_0)$ in the linear regime, which is consistent with the observations of Sec. IV. This occurs because although CS amplitude birefringence is proportional to distance [see e.g., Eq. (48)], the dominant source of error also grows with distance. Therefore, to leading order, any single, short GRB observation consistent with pure GR translates into upper limits on $\dot{\theta}_0 - \dot{\theta}_o/H_0$ that are *independent* of distance and depend only on the absolute detector sensitivity along the line of sight [Eq. (52)]². On the other hand, in the *non-linear* regime, where resonant behavior is present and the linear approximation is not valid, the blue shaded region in Fig. 2 does depend strongly on source distance.

B. Suboptimal Strategy

The previous analysis assumed the entire signal, including its narrow resonantly amplified contributions, are correctly identified through an appropriate, parity-violating template and summed in phase to extract the relevant signal power ρ . In other words, in the previous subsection we assumed a follow-up of each detected signal with a family of CS parity-violating, resonantly-amplified templates possessing two additional parameters $(f_{p,s}, f_{p,0})$ or equivalently $(\dot{\theta}_0, \ddot{\theta}_0)$. In this section, we investigate constraints on parity violation if all matched filtering is performed with parity-preserving, GR templates.

Given a GW detection, matched filtering with GR templates will return a set of best-fit parameters $\tilde{\lambda}_{\text{GR}}$ that maximize the SNR ρ_{max} . In the absence of noise, the values of $(\dot{\theta}_0, \ddot{\theta}_0)$ that lead to $\tilde{\rho} = \rho_{\text{max}}$ are simply those on the diagonal of Fig. 2, i.e., $\ddot{\theta}_0 = H_0 \dot{\theta}_0$. In the presence of noise, however, random fluctuations in the amplitude can resemble a resonant amplification. Therefore, one can search for the largest values of $(\dot{\theta}_0, \ddot{\theta}_0)$ that lead to a $\tilde{\rho}$ that is consistent with ρ_{max} . Such values of $(\dot{\theta}_0, \ddot{\theta}_0)$ then serve as an upper limit or constraint on the magnitude of parity violation in the signal.

Such a study leaves out the fact that a GR matched filtering calculation unavoidably induces a fundamental error in the estimation of GR parameters, if the signal is

² As in the linear case, the expression $\langle v \rangle < 1/\rho$ misleadingly suggests distance-dependent results. Areas in Fig. (2) only apply to self-consistent choices for ρ and D . For example, the contour for $|\mathcal{G} - 1| < 2/10$ at $D = 600\text{Mpc}$ corresponds to either twice as sensitive an instrument or $2^{6/5}$ times larger a binary chirp mass.

parity violating. This is a manifestation of fundamental bias [45]. In other words, the true physical parameters of the signal $\vec{\lambda} = \vec{\lambda}_{\text{GR}} + \delta\vec{\lambda}$, where $\delta\vec{\lambda}$ is the aforementioned error. We shall here ignore this error and leave an investigation of fundamental bias to a future publication.

As in the previous subsection, given a source with $|\xi| = 1$ and a single detector, we cannot distinguish between a purely right or purely left circularly-polarized signal, and thus, the SNR $\tilde{\rho}$ we would detect is

$$\tilde{\rho} = 4 \int_0^\infty df \frac{|\tilde{h}_{GR}|^2}{S_h(f)} \text{Re} \left[\frac{\mathcal{F}_{\text{R,L}}(\eta_s, k)}{\mathcal{F}_{\text{R,L}}(\eta_0, k)} \right]^{1/2} \equiv \hat{\rho} \tilde{\mathcal{G}}_{\text{R,L}} \quad (73)$$

where

$$\tilde{\mathcal{G}}_{\text{R,L}} \equiv \frac{1}{I_7} \int_0^\infty df \frac{f^{-7/3}}{S_h(f)} \text{Re} \sqrt{\frac{1 - f/(a_s f_{p,s})}{1 - f/(a_0 f_{p,0})}}. \quad (74)$$

Notice that we have here crudely assumed the resonantly amplified waveform is projected onto a pure GR signal model with identical parameters. To improve the realism of this calculation, one could maximize over time and phase of coalescence, but we shall not do this here.

Unlike the intrinsic SNR of the previous subsection, the integral defining $\tilde{\rho}$ requires no regularization. This is because $\tilde{\mathcal{G}}_{\text{R,L}}$ differs from $\mathcal{G}_{\text{R,L}}$ in that the former contains a square root, while the latter contains an absolute value. This square root leads to a well-defined integral, as we explore in more detail in the Appendix. All other details of the numerical implementation are the same as in the previous subsection.

When resonant frequencies are very large (i.e., in the linear regime, where constraints on θ' are weak), then Eq. (74) reduces to

$$\tilde{\mathcal{G}} \approx 1 + \frac{\lambda_{\text{R,L}}}{2} \langle v \rangle, \quad (75)$$

which is precisely half the amplification seen using an optimal signal model in the previous subsection. We have computed figures similar to Fig. 2 and we indeed find that the constraints quoted in the previous subsection deteriorate at most by a factor of 2. Of course, when one maximizes over extrinsic and intrinsic parameters, the match will increase, and thus the constraints will improve.

VI. EXTENSION AND DISCUSSION

In this section we discuss estimates of various factors that improve the order of magnitude results from the previous section. We also discuss limiting noise sources that could potentially deteriorate the constraints.

A. Constraints from single short GRBs

A network of N_d GW detectors using coherent data analysis is more sensitive than one detector by a factor

$\sqrt{N_d}$ in ρ , neglecting differences in orientation and noise spectrum. The four-detector LIGO-Virgo network thus gains about a factor of 2 for a typical sky position, though the full beam pattern is complicated [46, 48]. Moreover, this network also is more robust than a single detector if the GRB is viewed off-axis [33, 34].

A BH/NS merger takes advantage of the mass dependence of the threshold (51), $\mathcal{M}^{5/6}$, which goes as the square root of the total mass. Thus a $30 M_\odot$ BH ($\mathcal{M} = 4.7 M_\odot$) would improve the threshold further by a factor of about 4. Above $30 M_\odot$ the improvement drops because the system starts merging before the frequency has swept through the LIGO band and because our analysis assumes no spin-orbit precession. If the BH is rapidly spinning and that spin is misaligned with the orbit, precession will lead to a time-dependent left/right polarization ratio, reducing ρ from the on-axis case and complicating the analysis. Spin-orbit misalignment could be large for dynamically-formed binaries. In BH-NS binaries formed from isolated binary evolution, spin and orbital angular momenta should usually be aligned and precession should be relatively unimportant; see e.g., Fig. 6 in [49].

Observations and population arguments suggest that GRB associated with NS/NS mergers have a narrow but nonzero range of opening angles; population arguments suggest narrow jets $\sigma_{\xi^2} = 0.02$ [50], while the lack of jet breaks in afterglows suggests that some jets may be as wide as 25° [51] (which is still $\xi \approx 0.9$). The finite collimation angle of the GRB will lead to a distribution of ξ^2 which will degrade the threshold if $\sigma_{\xi^2} \approx 1/\rho$ since σ_{ξ^2} adds roughly in quadrature with σ_D/D . Additionally, because $\xi^2 < 1$, these unknown angles can only reduce ρ , not increase it, introducing a weak negative bias towards smaller amplitudes. Without independent direct or a priori constraints on ξ , any short GRB amplitude measurement by itself can only constrain the particular combination $\lambda_{\text{R,L}} \langle v \rangle + (\lambda_{\text{R,L}} \xi - 1)$, as

$$\frac{\rho}{\hat{\rho}(\xi)} \approx 1 + \lambda_{\text{R,L}} \langle v \rangle \left[1 - \frac{1}{2} \frac{F_+^2 - F_\times^2}{F_+^2 + F_\times^2} (\lambda_{\text{R,L}} - \xi)^2 + O(\lambda_{\text{R,L}} - \xi)^3 \right], \quad (76)$$

where we have explicitly expanded Eq. (44) for a nearly face on, right- or left-handed source $\xi \approx \lambda_{\text{R,L}}$ and used that $\hat{\rho}(\xi) \sim \hat{\rho}(\lambda_{\text{R,L}})[1 + \lambda_{\text{R,L}}(\xi - \lambda_{\text{R,L}})]$. In practice, however, the LIGO-Virgo network (or any network of differently aligned detectors) is sensitive to both GW polarizations, and by projecting directly onto a circularly-polarized basis, this network can directly constrain $1 - \xi \simeq O(1/\rho)$. [A similar effect was observed in Seto [33] and Dalal et al. [34], where the LIGO-Virgo network (or any network of differently aligned detectors) can reduce the systematic errors in distance measurement to short GRBs induced by wide jets.] The net effect of a narrow distribution in ξ is therefore simply to weaken any single-observation constraint on $\langle v \rangle$ by roughly a factor of 2, from $1/\rho$ to $O(2)/\rho$.

Another source of error is due to mismodeling of the signal because of the neglect of higher harmonics present for example in PN amplitude corrections [52]. Such corrections appear in the stationary-phase of the Fourier transform as modifications to the amplitude of the form $\mathcal{A} \rightarrow \mathcal{A} (1 + \zeta_{1/2} u^{1/3} + \zeta_1 u^{1/3} + \zeta_{3/2} u)$, where $u = 2\pi M f$ is the reduced GW frequency and ζ_n are n th order PN amplitude coefficients, which depend on the mass ratio, the inclination angle and the polarization angles. Notice that the 1.5PN correction, ζ_3 , is proportional to f , which immediately suggests a strong-correlation and degeneracy with CS amplitude birefringence. This degeneracy should be affect the constraints quoted above much because the mass ratio is primarily determined by the phase at 1PN order, while $\langle v \rangle$ does not enter the phase at all. A full study of such possible degenerate behavior would require a full Fisher or Bayesian analysis that we shall carry out elsewhere.

The electromagnetic determination of the distance to the GW/GRB also has errors. The latest augmented WMAP results [53] imply $H_0 = 70.4 \pm 1.3 \text{ km s}^{-1} \text{ Mpc}^{-1}$ at 95% confidence. The intrinsic uncertainty in the Hubble constant translates to a relative distance uncertainty of roughly $\delta H_0 = 1.3/70.4 \lesssim 1.8\%$, far below the intrinsic SNR uncertainty $2/\rho$ for all but extremely bright sources ($\rho \gtrsim 108$). Peculiar velocities of host galaxies, internal orbital velocities within galaxies and galaxy clusters, and kick velocities of binaries due to supernova kicks should all be well under $1500 \text{ km/s} \simeq 0.005c$ [54], corresponding to a distance error of about 6% in a Hubble redshift of $z = 0.08$. Only for extremely bright sources or very close double NS binaries will non-cosmological velocities produce a noticeable error.

A more significant and less well controlled distance error arises through the redshift determination process itself. Currently short GRB distances can be estimated only through the redshift to electromagnetically associated hosts, and therefore depends critically on correct host identification [55–57]. For moderate to high redshift sources, particularly where short GRBs are assumed ejected from their putative host galaxy, associations and therefore redshift measurements could be significantly confused [58]. Fortunately, for the distances to which even advanced gravitational detectors are sensitive, relatively few galaxies can conceivably be associated with a coincident gravitational and electromagnetic signature (i.e., adopting a fiducial galaxy density $n_{gal} = 0.01 \text{ Mpc}^{-3}$, the number of galaxies in the electromagnetic sky-position angular extent θ and radial extent D error cone is of order $n_{gal} D^3 \pi \theta^2 / 3 = \mathcal{O}(1)$ for $D = 600 \text{ Mpc}$ and $\theta \simeq 1 \text{ arcmin}$). We therefore assume any future coincident short GRB and GW signal arising within $z < 0.4$ will have a correct host association and therefore a reliable redshift measurement.

Let us then summarize the enhancement and deterioration factors we have just discussed. A network of N_d detector enhances the bound by a factor of $\sqrt{N_d}$, while a BH/NS event enhances the constraint by a factor of

4. On the other hand, an unknown jet width deteriorates the constraint by a factor of 2, while a suboptimal search strategy also worsens the bound by a factor of 2. Putting all of these together, we expect a modification of the constraints quoted earlier by a factor of $1/\sqrt{N_d}$ for a NS/BH event or $4/\sqrt{N_d}$ for a NS/NS event (i.e., from $\langle v \rangle < 1/\hat{\rho}$ to $1/(\hat{\rho}\sqrt{N_d})$ for a NS/BH event, where $\hat{\rho}$ is the single-detector SNR).

Putting all of this together, we arrive at the following constraints. A single detector with advanced LIGO sensitivity measuring a non-resonant, NS/NS inspiral signal seen directly overhead with unknown jet width leads to a 1σ constraint of $|\dot{\theta}_0 - \ddot{\theta}_0/H_0| \leq 2400 \text{ km}$. A four-detector network would improve this limit to $|\dot{\theta}_0 - \ddot{\theta}_0/H_0| \leq 1200 \text{ km}$. A BH-NS merger, seen at comparable sensitivity over a longer baseline, would reduce the limit to $|\dot{\theta}_0 - \ddot{\theta}_0/H_0| \leq 300 \text{ km}$. All of this has assumed an optimal search strategy, but with a suboptimal one, i.e., using pure-GR templates, one would only reach a bound of $|\dot{\theta}_0 - \ddot{\theta}_0/H_0| < 600 \text{ km}$ for BH/NS events or $< 2400 \text{ km}$ for NS/NS ones.

Since the maximum $(\dot{\theta}_0, \ddot{\theta}_0)$ allowed by these bounds would lead to a resonance in band, the absence of such a resonance could allow $(\dot{\theta}_0, \ddot{\theta}_0)$ to be constrained much better. In fact, this could constrain $|\dot{\theta}_0 - \ddot{\theta}_0/H_0| \leq 50 \text{ km}$ to 1σ assuming an optimal search strategy (see e.g., Fig. 2 for 2σ constraints). If we additionally assume a four-detector coincident GW/GRB measurement of a NS/BH signal, the absence of a resonance could lead to a bound of³ $|\dot{\theta}_0 - \ddot{\theta}_0/H_0| \leq 25 \text{ km}$, even allowing for an unknown jet width and a suboptimal search strategy.

B. Population constraints

Combining N_0 GW/GRB observations will improve the CS threshold roughly as $\sqrt{N_0}$. Birefringence would manifest as a *bimodal distribution* of $\rho/\hat{\rho}$, with peaks on either side of unity. If GRB jets are poorly collimated, both peaks of the distribution of $\hat{\rho}/\rho$ would be smeared downward due to the distribution of ξ (see above).

Advanced detectors will observe very many short GRBs with GW associations. Roughly $R_{sky} \simeq 100 - 200$ short GRBs occur on the sky per year that produce enough flux to be detected by the current generation of satellites [59–61]. As a first approximation, host associations suggest that the *satellite-detected* short GRB population is roughly linearly distributed in redshift out to $z \simeq \mathcal{O}(1)$ [56, 59, 61, 62]. Therefore, adopting an

³ This constraint is an optimistic one, since if this bound is saturated, the resonance occurs near 2 kHz. At such high frequencies our calculations is limited by systematic errors due to incorrect waveform modeling, since one should in principle include the plunge and merger parts of the waveform in the modeling as well.

isotropic network horizon⁴ distance $D_{gw} > 200\text{Mpc}$, large enough to enclose many binary mergers per year, roughly

$$\begin{aligned} R_{gw+GRB} &\simeq \frac{f_{sky}}{z_{max}} D_{gw} H_0 R_{sky}, \\ &\simeq \frac{20}{\text{yr}} \frac{f_{sky}}{z_{max}} \frac{D_{gw}}{445 \text{ Mpc}} \frac{R}{200 \text{ yr}^{-1}} \end{aligned} \quad (77)$$

satellite-detected short GRBs could be detected by a GW interferometer network. Even under more conservative assumptions including the local event rate and expected beaming angles, a significant number of NS-NS or BH-NS binaries should be coincident with a short GRB event: more than $> O(10\%)$ of all GW detections. Given the latest event rate predictions [65, 66], at least 2 should be detected per year. To summarize, a population of at least 4 short GRBs could improve constraints on $\dot{\theta}_0$ by a factor $\sqrt{4} = 2$.

Combining this factor of two and those of the previous subsection, we find that parity violation could be constrained to the level of $\langle v \rangle < 1/(\hat{\rho}\sqrt{N_d N_0})$ for a NS/BH event. Modeling parity violation with CS gravity and first adopting a non-resonant parity-violating event, it is reasonable to expect that after two calendar years (the length of the LIGO S5 run) an advanced LIGO-Virgo network operating in coincidence with GRB observatories would yield a 1σ confidence detection of or upper limit on $|\dot{\theta}_0 - \dot{\theta}_o/H_0|$ of 150 km for BH-NS (600 km for NS-NS) using optimally matched templates, or 300 km for BH-NS (1200 km for NS-NS) using a conventional pure-GR data analysis strategy. Again, as the maximum $(\dot{\theta}_0, \dot{\theta}_o)$ allowed by the aforementioned constraints would lead to a resonance in band, the absence of resonances could allow a much better constraint. In the neighborhood of $\dot{\theta}_0 = 0$, the absence of such resonance could yield a bound on $\dot{\theta}_0$ of $\mathcal{O}(10 \text{ km})$.

The projected constraints on CS gravity can be thus more than an order of magnitude better than current Solar System bounds placed with the LAGEOS satellites [38]. Although none of these constraints are competitive with the one recently placed with the double binary pulsar [39], the latter only samples parity violation in the neighborhood of this binary, while the Solar System one is sensitive to parity violation only in the vicinity of the Earth-Moon system. The test proposed here would allow for constraints of the dynamical sector of parity violating theories along the GW geodesic, thus exploring a much larger region of the Universe.

⁴ Because each short GRB is presumed optimally oriented, the range to which it can be detected is significantly greater than the angle-averaged range to which a typical source could be observed. In practice, the distance to which short GRBs could be detected will be greater still, because when a shorter stretch of data is searched, the detection threshold can be set significantly lower [63, 64].

C. Temporal-Spatial Variability of Parity Violation

In this paper, we have proposed limits on $\dot{\theta}_0$ and $\ddot{\theta}_0$ assuming (i) that θ varies on cosmological timescales and (ii) homogeneously and isotropically throughout the Universe. In principle, neither assumption need apply, as the θ field that parametrizes parity violation in CS gravity should be prescribed by the more fundamental theory of which CS gravity is only an effective model. If the θ field does not obey the symmetries of the background (homogeneity and isotropy in the cosmological case), then the background metrics employed, on which GW propagate, need not be solutions to the effective theory. More general θ fields would possibly require a re-analysis of the appropriate cosmological solutions and the propagation of GWs in them.

With this caveat in mind, the more generic expressions of Eq. (29) that parameterize generic parity violating effects via the amplification process of Sec. V suggest that the proposed constraints are primarily on a ratio of $\mathcal{F}_{\text{R,L}}$, with one factor at the source (the numerator) and another, more critical one at the detector (the denominator). These two factors can be separated. For example, the resonant frequency and resonant bandwidth in our detectors are set primarily by the present-day evolution of θ . If a resonance is indeed in band, *every* source with some amount of resonant polarization will be amplified roughly the same way; stacking power from multiple detections could constrain the presence of a universal spectral feature and potentially directly constrain $\dot{\theta}_0$, independent of its cosmological behavior, to lie outside the wavelength region to which LIGO is sensitive. On the other hand, the difference between the values of $\dot{\theta}$ at present and the source determine how close a zero in the numerator is to the resonance and thus the amplification $\mathcal{G}_{\text{R,L}}$; cf. Eq. (65). Therefore, if the detected SNRs do exhibit some amplifications $\rho/\hat{\rho}$ versus D that are *not* roughly uniformly increasing with distance, these measurements can be fit to either a functional form (if the points trace a curve) or a distribution (if the points have excess scatter) for $\dot{\theta}$. As a concrete example, so long as resonances are at frequencies far higher than in band ($\kappa\theta' \ll 1$) and the source is at low enough redshift that cosmological terms can be ignored ($a = a_s \approx 1$), the relative amplification in SNR due to CS birefringence is [cf. Eq. (21)]

$$\rho/\hat{\rho} \approx 1 + \lambda_{\text{R,L}} \pi \langle f \rangle (\theta'_0 - \theta'_s), \quad (78)$$

which applies to any $\theta'(\eta)$ which varies on scales faster than cosmological timescales. This would then allow for generic tests of gravitational parity violation, irrespective of the specific theoretical model.

Acknowledgments

We thank D. Fox and M. C. Miller for helpful discussions and N. Cornish for helpful comments on the

manuscript. This work was supported by NSF grants PHY-0555628, PHY-0748819, and PHY-0855589, and by the Center for Gravitational Wave Physics under NSF cooperative agreement PHY-0114375. N.Y. was supported by National Science Foundation award PHY-0745779. R.O. was supported by National Science Foundation award PHY 0653462 and the Center for Gravitational Wave Physics. S.A was supported by NSF Grant PHY-0901925. B.J.O. was also supported by the LIGO Visitors Program. LIGO was constructed by the California Institute of Technology and Massachusetts Institute of Technology with funding from the National Science Foundation and operates under cooperative agreement PHY-0107417. This paper has been assigned LIGO Document Number P1000051.

Appendix: Singular Behavior and Resonances in CS Gravitational Waves

Parity violating GWs need not present a pole in the frequency domain, but the theory we use to exemplify such violation, CS gravity, does. As shown in Sec. II, such singularities arise due to poles in the modified field equations, i.e., Eqs. (10) and (13). The effect of such singularities was analyzed in Sec. V where it was seen to lead to a resonant magnification or amplification of the SNR. That section, however, does not explain why such amplification is finite; this is the topic of this appendix. We begin with a basic introduction to resonances and the non-uniform validity of perturbation theory, as this topic may be unfamiliar to the GW community, following mostly [67]. We then proceed to the study of singularities in CS gravity, their characterization and treatment.

1. Resonances and the Nonuniform Validity of Perturbative Expansions

Consider the differential equation for a driven harmonic oscillator

$$\ddot{y} + y = \cos \omega t, \quad (\text{A.1})$$

whose solution is

$$y(t) = A \cos t + B \sin t + \frac{\cos \omega t}{1 - \omega^2}. \quad (\text{A.2})$$

This solution is valid only when $|\omega| \neq 1$, as in the limit $\omega \rightarrow 1$, the oscillator absorbs large quantities of energy and the amplitude of the oscillations grow unbounded. The solution to Eq. (A.1) at resonance ($|\omega| = 1$) is

$$y = A \cos t + B \sin t + \frac{t}{2} \sin t \quad |\omega| = 1. \quad (\text{A.3})$$

Notice that the divergent term has been replaced by a regular, *secular* contribution. Such a secular term grows with time and is unbounded in the limit $t \rightarrow \infty$, as then the oscillator absorbs energy without limit.

The emergence of secular terms in the solution to certain differential equations signals the breaking of uniform perturbation theory. In order to exemplify this concept in more detail, consider Duffing's differential equation

$$\ddot{y} + y + \epsilon y^3 = 0, \quad (\text{A.4})$$

with $\epsilon \ll 1$ and the boundary conditions $[y(0), \dot{y}(0)] = [1, 0]$. Although the ϵy^3 term cannot be interpreted as a driving force with a certain natural frequency, we shall show next that its perturbative solution unavoidably introduces secular growth, just as in the case of the driven harmonic oscillator at resonance.

Let us assume the following perturbative ansatz for the solution to Duffing's equation

$$y(t) = \sum_{n=0}^{\infty} \epsilon^n y_n(t). \quad (\text{A.5})$$

Order by order in multiple scale analysis, Duffing's equation becomes $\ddot{y}_0 + y_0 = 0$ to $\mathcal{O}(\epsilon^0)$, and $\ddot{y}_1 + y_1 = -y_0^3$ to $\mathcal{O}(\epsilon)$. The solution to the zeroth-order equation that satisfies the above initial conditions is simply $y_0(t) = \cos t$. The solution to the first-order equation that satisfies the same initial conditions leads to the full solution

$$y(t) = \cos t + \left[\frac{1}{32} (\cos 3t - \cos t) - \frac{3t}{8} \sin t \right] \epsilon + \mathcal{O}(\epsilon^2). \quad (\text{A.6})$$

Notice that a secular term has appeared in the first-order solution, i.e., the last term inside the square-brackets is unbounded as $t \rightarrow \infty$. This solution is valid to $\mathcal{O}(\epsilon^2)$ for fixed t , but as one considers times $t = \mathcal{O}(1/\epsilon)$ or larger, Eq. (A.6) ceases to be valid.

The non-uniform validity of the perturbative solution leads to an inaccurate approximation to the exact solution at late-times, as the exact solution is actually bounded for all times. To show this, one can construct an *energy integral* and show that it is bounded. In the case of Duffing's equation, one can multiply Eq. (A.4) by \dot{y} and then rewrite it as

$$\frac{1}{2} \dot{y}^2 + \frac{1}{2} y^2 + \frac{1}{4} \epsilon y^4 = C, \quad (\text{A.7})$$

after one time integration with constant C . Equation (A.7) can be thought of as a closed bounded orbit in the phase space with coordinates (y, \dot{y}) . Due to the initial conditions, one easily finds that $C = (2 + \epsilon)/4$. Since each term on the left-hand side is positive if $\epsilon > 0$, then $y^2 < 2C$ and y is bounded by $y < (1 + \epsilon/2)^{1/2}$. We have thus proved that although the perturbative solution presents divergent behavior at late times due to the secular term arising at resonance, the exact solution is properly bounded. Another way to show this is to partially sum all the divergent, secular terms in the perturbative solution. In the case of Duffing's equation, one would find that these terms sum up to $\cos[t(1 + 3\epsilon/8)]$, which is properly bounded at $t \rightarrow \infty$.

This subsection has taught us several important lessons. Resonant solutions to differential equations can be studied close to their singularities via perturbation theory. Such a study might reveal secular growth in the perturbative solutions, but this does not mean that the solution, or the theory from which this derives, is unstable. Instead, such unbounded growth is an indication that the perturbative solution has a non-uniform region of validity. The construction of positive energy integrals allows us to prove that solutions are bounded from above, and that secular growth is artificial.

2. Boundedness of CS Resonances

Let us now consider the resonant structure of the CS differential equations for wave propagation and their perturbative solution. In Sec. II we found that the differential equations for CS phase evolution have a singular driving force, i.e., the right-hand sides of Eqs. (10) and (13) diverge in the limit $\lambda_{\text{R,L}} k \dot{\theta} \rightarrow 1$. Later in Sec. III we found that the exact solution to these differential equations are also singular in this limit, i.e., Eq. (28) diverges as $\mathcal{S}_{\text{R,L}} \rightarrow 0$.

The perturbative, approximate solutions to the singular CS phase evolution equations are in fact regular, although they lead to secular growth. This can be seen from Eqs. (16) and (17), which are proportional to the GW travel time, or equivalently distance, so that as $t \rightarrow \infty$, the perturbative solution is unbounded. Such secular growth is nothing but an indication of the non-uniform validity of the perturbative solution. In fact, from the structure of Eqs. (16) and (18), we can deduce that the approximation ceases to be valid when the GW has travelled a distance $D = \mathcal{O}(f_0^{-1} \dot{\theta}_0^{-1})$ or $D = \mathcal{O}(f_0^{-1} H_0^{-1} \dot{\theta}_0^{-1})$.

Let us now try to show boundedness of the solution through the construction of an energy integral. Equation (24) can be rewritten as

$$h''_{\kappa} + 2 \frac{d}{d\eta} (\ln \mathcal{S}_{\text{R,L}}) h'_{\kappa} + \kappa^2 h_{\kappa} = 0. \quad (\text{A.8})$$

For simplicity, we take h to be real and multiply the above equation by h' . Integrating once we find

$$(h'_{\kappa})^2 + 4 \int (h'_{\kappa})^2 \left[\frac{d}{d\eta} (\ln \mathcal{S}_{\text{R,L}}) \right] d\eta + \kappa^2 h_{\kappa}^2 = 2C. \quad (\text{A.9})$$

Choosing initial conditions $h_{\kappa}(0) = 1$ and $h'_{\kappa} = 0$, we find that $C = \kappa^2/2 \geq 0$. It then follows that the solution is bounded from above by

$$h_{\kappa} < \sqrt{1 - \frac{4}{\kappa^2} \int (h'_{\kappa})^2 \left[\frac{d}{d\eta} (\ln \mathcal{S}_{\text{R,L}}) \right] d\eta} \quad (\text{A.10})$$

provided the modified scale factor is positive:

$$\frac{\mathcal{S}'_{\text{R,L}}}{\mathcal{S}_{\text{R,L}}} = \frac{\dot{\mathcal{S}}_{\text{R,L}}}{\mathcal{S}_{\text{R,L}}} = \frac{1}{2} \frac{2H - \lambda_{\text{R,L}} k (\ddot{\theta} + H\dot{\theta})}{1 - \lambda_{\text{R,L}} k \dot{\theta}} > 0. \quad (\text{A.11})$$

The positivity of the effective Hubble parameter $\dot{\mathcal{S}}_{\text{R,L}}/\mathcal{S}_{\text{R,L}}$ depends on the size of $\dot{\theta}$. This quantity is indeed positive when $\dot{\theta} = 0 = \ddot{\theta}$ and the universe is expanding such that $H > 0$. Moreover, this quantity is also positive away from the resonance, i.e., if $\dot{\theta} \ll \lambda_{\text{R,L}}/k$, as then the CS modification is a small deformation of the GR result. At resonance, ($\dot{\theta} = \lambda_{\text{R,L}}/k$, $\ddot{\theta} = 0$), the positivity of $\dot{\mathcal{S}}_{\text{R,L}}/\mathcal{S}_{\text{R,L}}$ depends on whether $\dot{\theta}$ approaches $\lambda_{\text{R,L}}/k$ from below or above. If approached from below, $\dot{\theta} = \lambda_{\text{R,L}}(1 - |\epsilon|)/k$ as $\epsilon \rightarrow 0_+$, then $\dot{\mathcal{S}}_{\text{R,L}}/\mathcal{S}_{\text{R,L}} > 0$, while the opposite is true if approached from above, $\dot{\theta} = \lambda_{\text{R,L}}(1 + |\epsilon|)/k$ as $\epsilon \rightarrow 0_+$.

For strong CS parity violation, i.e., $\dot{\theta} > \mathcal{O}(1/k)$, $\dot{\mathcal{S}}_{\text{R,L}}/\mathcal{S}_{\text{R,L}} > 0$ for all $\dot{\theta} \geq 2\lambda_{\text{R,L}}/k$, but we cannot prove the solution is bounded via this energy integral method if $\lambda_{\text{R,L}} k \dot{\theta}$ is in the interval $[1, 2]$. A full treatment of strong CS parity violation, however, requires that one includes higher-order θ -interactions in the action, as Eq. (3) is an *effective* theory valid in the weak coupling limit only. Such interactions will contribute to the energy integral, particularly in the strong coupling limit. Since we do not have a higher-order completion of CS gravity, we cannot prove boundedness in this limit.

In spite of the apparent secular growth of the perturbative solution in the weak CS coupling limit, we have here shown that the exact solution remains bounded in this limit. The secular growth observed is then nothing but an artifact of the perturbative expansion and should not be seen as an indication of an instability in the theory.

3. Trans-Singular CS Resonances

Proving that the exact solution to the CS phase evolution equation remains bounded does not tell us how to deal with its singularity. However, as in the case of the driven harmonic oscillator of Eq. (A.1), the solution we found away from resonance is not valid at resonance. In order to find the solution close to the singularity, we must solve the phase evolution equation perturbatively, restricting attention to a neighborhood close to the pole.

The general form of a parity violating wave equation

$$h''_{\text{R,L},\kappa} + \kappa^2 h_{\text{R,L},\kappa} + \frac{\mathcal{F}'_{\text{R,L}}}{\mathcal{F}_{\text{R,L}}} h'_{\text{R,L},\kappa} = 0 \quad (\text{A.12})$$

has a pole when $\mathcal{F}_{\text{R,L}}$ vanishes. Equation (A.12) is nothing but Eq. (22) with the replacement $\mathcal{H} \rightarrow \mathcal{S}'_{\text{R,L}}/\mathcal{S}_{\text{R,L}} \equiv \mathcal{F}'_{\text{R,L}}/(2\mathcal{F}_{\text{R,L}})$, where we recall that the squared amplitude $\mathcal{F}_{\text{R,L}} \equiv \mathcal{S}_{\text{R,L}}^2$. With this notation, recall that in CS gravity $\mathcal{F}_{\text{R,L}} \equiv a^2 - \lambda_{\text{R,L}} \kappa \theta'$. Let us linearize the source function $\mathcal{F}_{\text{R,L}}$ about the (κ -dependent) conformal pole $\eta_p(\kappa)$, defined via $a^2(\eta_p) - \kappa \theta'(\eta_p) = 0$, though the Taylor expansion $\mathcal{F}_{\text{R,L}} = \mathcal{F}_{\text{R,L}}|_p + \mathcal{F}'_{\text{R,L}}|_p(\eta - \eta_p)$, where the vertical bar stands for evaluation at the pole. Equation (A.12) simplifies to a Bessel equation

$$h''_{\text{R,L},\kappa} + (\eta - \eta_p)^{-1} h'_{\kappa} + \kappa^2 h_{\text{R,L},\kappa} = 0. \quad (\text{A.13})$$

Notice that by linearizing about $\eta = \eta_p$ we have lost the distinction between left and right-polarized waves, as the $\lambda_{\text{R,L}}$ dependence in the source term appears only at second order in the Taylor expansion.

Solutions to this wave equation linearized about the pole can be straightforwardly obtained as a superposition of Hankel functions. Imposing a no-incoming-radiation boundary condition at infinity, the solution reduces to the outward propagating, cylindrical wave solution

$$h_{\text{R,L},\kappa}(\eta) = \mathcal{C} H_0^{(1)}[\kappa(\eta - \eta_p)], \quad (\text{A.14})$$

where \mathcal{C} is a normalization constant. The quantity $H_0^{(1)}$ is a Hankel function of the first kind, not to be confused with the Hubble parameter at present time. Notice that this solution is discontinuous and singular at $\eta = \eta_p$, a conformal time often reached after propagation on cosmological scales. Guided by analytic continuation, by conserved current across the singularity (the Wronskian of Eq. (A.13)), and by the need for a nearly-Minkowski gravitational propagator in the neighborhood of $\eta \approx \eta_p(f)$, we adopt this particular solution on both sides of the resonance.

One can reinterpret the solution in terms of propagators. In the neighborhood of some η_s , e.g., near the source, each spatial Fourier component is evolved forward with a simple scalar propagator:

$$h_{\text{R,L},\kappa}(\eta) = K_\kappa(\eta, \eta_s) h_{\text{R,L},\kappa}(\eta_s), \quad (\text{A.15})$$

$$K_\kappa(\eta, \eta_s) \equiv \frac{H_0^{(1)}[\kappa(\eta - \eta_p)]}{H_0^{(1)}[\kappa(\eta_s - \eta_p)]}. \quad (\text{A.16})$$

The functional form of this equation resembles the solution to the differential equations of para-axial optics, where as initial data we require only the initial state $h_{\text{R,L},\kappa}(\eta_s)$. In fact, except for a fraction of a wavelength in the neighborhood of the pole $\eta \approx \eta_p$, the propagator can be well-approximated at late times by

$$K_\kappa(\eta, \eta_s) \approx \sqrt{\frac{\eta_s - \eta_p}{\eta - \eta_p}} e^{-i\kappa(\eta - \eta_s)}, \quad \kappa(\eta - \eta_p) \gg 1, \quad (\text{A.17})$$

which can be obtained by either expanding the Hankel functions in $\kappa(\eta - \eta_p) \gg 1$ or solving Eq. (A.13) in this limit.

The functional form of the propagator in terms of the source function $\mathcal{F}_{\text{R,L}}$, namely

$$K_\kappa(\eta, \eta_s) \approx \sqrt{\frac{\mathcal{F}_{\text{R,L}}(\eta_s)}{\mathcal{F}_{\text{R,L}}(\eta)}} e^{-i\kappa(\eta - \eta_s)} \quad (\text{A.18})$$

was already derived in Sec. III. Taylor expanding the source function about resonance

$$\mathcal{F}_{\text{R,L}}(t) \sim 1 - \lambda_{\text{R,L}} k_p \dot{\theta} - \lambda_{\text{R,L}} k_p \ddot{\theta}(t - t_p) = -\lambda_{\text{R,L}} k \ddot{\theta}(t - t_p), \quad (\text{A.19})$$

where in the second equality we have used the resonance condition $\dot{\theta} = \lambda_{\text{R,L}}/k$, we find that Eq. (A.18) reduces

exactly to Eq. (A.17). Notice however that Eq. (A.18) is formally valid away from the pole, while the true representation of the solution close to the pole is given by Eq. (A.16).

All of these solutions diverge when $\eta = \eta_p$, but the width of the resonance is extremely narrow in frequency space. This width can be approximated as $\delta f_p \simeq \dot{f}_p \delta t_p$, which for a minimal-width wave packet with $\delta t_p \delta f_p \simeq 1$, implies $\delta f_p = \mathcal{O}(\dot{f}_p^{1/2})$. Using that $f_p = 1/(2\pi\dot{\theta})$ and $\dot{f}_p = -\ddot{\theta}/(2\pi\dot{\theta}^2)$, we find that $\delta f_p \approx \mathcal{O}[(H/\dot{\theta})^{1/2}]$, where we have assumed $\dot{\theta}$ evolves on cosmological scales $\ddot{\theta} = \mathcal{O}(H\dot{\theta})$. Evaluating these expressions today on Earth, we find that $\delta f_p = \mathcal{O}(10^{-8} \text{ Hz})$, where for $\dot{\theta}$ we have saturated the Solar System constraint $\dot{\theta} < 2000 \text{ km}$.

Although any *single, large-scale-coherent Fourier mode* is formally divergent, any finite-duration, band-limited waveform always remains finite. This is because to obtain any finite-duration waveform one must undo the Fourier decompositions performed in this paper [see e.g., Eq. (8) or Eq. (11)]. The reconstruction of the full waveform then requires the integration of $h_\kappa(\eta)$ over all wave-numbers:

$$\begin{aligned} h_{\text{R,L}}(\eta, \chi^i) &\equiv \frac{1}{(2\pi)^{3/2}} \int d\kappa h_{\text{R,L},\kappa}(\eta) e^{-i\kappa_i \chi^i}, \quad (\text{A.20}) \\ &= \frac{\mathcal{D}}{(2\pi)^{3/2}} \int d\kappa K_\kappa(\eta, \eta_s) \kappa^{-7/6} e^{-i\kappa(\chi - \eta_s)}, \end{aligned}$$

where \mathcal{D} is a new constant related to \mathcal{A} in Eq. (34), which depends on the chirp mass, inclination angle and distance to the source, and where we have assumed the wave propagates in the χ direction with conformal wavenumber κ . This integral can be split into three integrals: two pieces that avoid the singularity of the propagator close to the pole and one piece that integrates through this singularity. Clearly, the first two pieces are finite, while the last piece can be approximated using Eq. (A.16) in the neighborhood of the pole:

$$h_{p,\text{R,L}} \sim \frac{\mathcal{D}}{(2\pi)^{3/2}} \int_{\kappa_p^-}^{\kappa_p^+} d\kappa \frac{H_0^{(1)}[\kappa(\eta_0 - \eta_p)]}{H_0^{(1)}[\kappa(\eta_s - \eta_p)]} \frac{e^{-i\kappa(\chi - \eta_s)}}{\kappa^{7/6}}, \quad (\text{A.21})$$

where we have defined $\kappa_p^\mp = \kappa_p \mp 2\pi\epsilon$. An asymptotic expansion of the Hankel function about zero argument reveals that

$$H_0^{(1)}(x) \sim \text{sign}(x) + \frac{2i}{\pi} \left[\ln\left(\frac{|x|}{2}\right) + \gamma_E \right], \quad x \ll 1 \quad (\text{A.22})$$

where $\gamma_E = 0.5772157\dots$ is the Euler constant. Using this expansion, assuming the light-cone condition $\chi = \eta_s$, and pulling out of the integral all quantities that remain roughly constant near the pole, the integral of Eq. (A.21)

becomes

$$h_{p,R,L} \sim \frac{\mathcal{E}}{\kappa_p} \int_{\kappa_p^-}^{\kappa_p^+} d\kappa \left\{ \text{sign}(\kappa_p(\eta_0 - \eta_p)) + \frac{2i}{\pi} \left[\ln \left(\frac{|\kappa_p(\eta_0 - \eta_p)|}{2} \right) + \gamma_E \right] \right\} \\ \mathcal{E} \equiv \frac{\mathcal{D}}{(2\pi)^{3/2}} \frac{\kappa_p^{-1/6}}{H_0^{(1)}[\kappa(\eta_s - \eta_p)]}. \quad (\text{A.23})$$

Using $\eta_0 = \eta_p + \mathcal{R}(\kappa - \kappa_p)$, we find that the most divergent term of the above integral is proportional to

$$h_{p,R,L} \propto \mathcal{E} \frac{\epsilon}{\kappa_p} \ln(\kappa_p \mathcal{R} \epsilon) = \mathcal{E} \frac{\epsilon}{\kappa_p} \ln \left(\frac{\kappa_p \epsilon}{\delta \kappa_p^2} \right), \quad (\text{A.24})$$

where in the second relation we have used that $\mathcal{R} = \mathcal{O}(\delta \kappa_p^{-2})$. We have then proved that any finite-duration, band-limited waveform always remains finite, as $h_{p,R,L}$ remains finite when $\epsilon \rightarrow 0$. Furthermore, the contribution of the inverse Fourier transform near the pole is clearly subdominant: to use a numerical example, saturating the Solar System constraint $\dot{\theta}_0 = 2000$ km, such that $\kappa_p \sim 150$ Hz, and using a buffer of size $\epsilon = 10^{-8}$ Hz around the pole, then $h_p \leq 10^{-8} \mathcal{E}$.

One might worry that although the pole does not affect the waveform itself, it might affect the calculation of the SNR, as this depends on the integral of the square of the Fourier transform of the waveform. The *approximate* temporal-only Fourier transform of the propagator of Eq. (A.16) in the stationary phase approximation is

$$\tilde{K}_\kappa(\omega|\eta_0) \equiv \int d\eta K_\kappa(\eta, \eta_0) e^{i\omega\eta} \approx \sqrt{\frac{\mathcal{F}(\eta_0)}{\mathcal{F}(\eta_s)}} \delta(\omega - \kappa) e^{i\omega\eta_0}, \quad (\text{A.25})$$

where ω is conformal frequency. Then, the present-day temporal-only Fourier transform $\tilde{h}(\omega)$ can be expressed in terms of the spatial Fourier transform h_κ at the fiducial source time η_0 :

$$\tilde{h}(\omega) = \int \frac{d\kappa}{2\pi} \tilde{K}_\kappa(\omega) h_\kappa(\eta_0) e^{-i\kappa\chi}, \quad (\text{A.26})$$

where $\eta_0 - \eta_s = \chi$. Except for an extremely narrow neighborhood near $\eta_0 \neq \eta_p(f)$, the stationary phase propagator and thus this model for $\tilde{h}(\omega)$ is an excellent approximation. Substituting this expression into Eq. (30) for SNR gives the expression for resonant SNR adopted in the text [Eq. (60)].

As the denominator in the SNR inevitably includes a pole at the zero of \mathcal{F}_κ ($\kappa = \lambda_{R,L}/\theta'$), this approximate integral indeed formally diverges logarithmically. However, this logarithmic divergence arises by applying an approximate propagator and its Fourier transform outside of their domain of applicability. In the neighborhood of $f_{p,s}$, the relevant propagator is approximately Eq. (A.16), modulo higher-derivative corrections to \mathcal{F}'/\mathcal{F} [cf. Eqs. (A.12), (A.13)].

The temporal-only Fourier transform of the resonant propagator is proportional to the Fourier transform of the standard Hankel function, keeping in mind this Fourier transform (unlike many used in classical scattering problems) is over a two-sided argument:

$$\tilde{K}(\omega) = \int_{-\infty}^{\infty} e^{i\omega\eta} \frac{H_0^{(1)}[\kappa(\eta - \eta_p)]}{H_0^{(1)}[\kappa(\eta_s - \eta_p)]} d\eta, \\ = \frac{e^{i\omega\eta_0}}{\kappa} \frac{\tilde{H}_0^{(1)}(\omega/\kappa)}{H_0^{(1)}(\kappa(\eta_s - \eta_p))}, \quad (\text{A.27})$$

$$\tilde{H}_0^{(1)}(Y) \equiv \int_{-\infty}^{\infty} dX H_0^{(1)}(X) e^{iXY} \quad (\text{A.28})$$

The numerator, the Fourier transform $\tilde{H}_0^{(1)}$, is well-behaved and unaffected by the proximity of ω or κ to resonance ($\eta_0 = \eta_p(\kappa)$). The resonance condition enters only in the denominator. As $H_0^{(1)}(X)$ has no zeros for real X , however, the time-domain Fourier transform of the resonant propagator \tilde{K} and the transform of the amplified waveform $\tilde{h}(\omega)$ have no poles on the real axis. This shows that even if the calculation were done exactly, the true SNR would remain finite. Moreover, given the extremely slow rate at which the resonant frequency evolves, we can approximate $\tilde{H}_0^{(1)}(\omega/\kappa)$ as proportional to $\delta(\omega - \kappa)$. This implies that to a good approximation the Fourier transform of the *time dependent* propagator is $K_\kappa(\eta_0, \eta_s) \delta(\omega - \kappa)$.

With this reasonable approximations at hand, the SNR becomes

$$\rho_{R,L}^2 = 4 \int_0^\infty \frac{|\tilde{h}_{R,L}|^2}{S_h(f)} df = 4 \int_0^\infty \frac{|h_{R,L,\kappa}|^2}{S_h(\kappa)} d\kappa, \\ = \mathcal{D}^2 \int_0^\infty |K_\kappa(\eta_0, \eta_s)|^2 \kappa^{-7/3} \frac{d\kappa}{S_h(\kappa)}. \quad (\text{A.29})$$

As before, let us split this integral into three pieces: two of them that avoid the singularity and one that integrates through it. In the neighborhood of the singular point, we once more approximate the propagator using Eq. (A.16), so that

$$\rho_{R,L,p}^2 \simeq 4\mathcal{D}^2 \int_{\kappa_p^-}^{\kappa_p^+} \left| \frac{H_0^{(1)}[\kappa(\eta_0 - \eta_p)]}{H_0^{(1)}[\kappa(\eta_s - \eta_p)]} \right|^2 \kappa^{-7/3} \frac{d\kappa}{S_h(\kappa)}. \quad (\text{A.30})$$

Notice that the argument of the Hankel function function in the numerator is the only quantity that formally diverges at the pole, so let us now rewrite the integral as

$$\rho_{R,L,p}^2 \simeq \bar{\mathcal{E}} \int_{\kappa_p^-}^{\kappa_p^+} \left| H_0^{(1)}[\kappa_p(\eta_0 - \eta_p)] \right|^2 d\kappa, \\ \bar{\mathcal{E}} \equiv 4\mathcal{D}^2 \left| H_0^{(1)}[\kappa_p(\eta_s - \eta_p)] \right|^{-2} \frac{\kappa_p^{-7/3}}{S_h(\kappa_p)}, \quad (\text{A.31})$$

where we have pulled out several factors that are non-singular at the pole and roughly constant near the resonance. These expressions lead to singular results if

one evaluates it with the late-time expansion of the Hankel function of Eq. (A.17). Instead, using the small-argument Hankel function expansion provided in Eq. (A.22), the SNR integral becomes

$$\rho_{\text{R,L},p}^2 \simeq \bar{\mathcal{E}} \int_{\kappa_p^-}^{\kappa_p^+} \left\{ \text{sign}[\kappa_p \mathcal{R}(\kappa - \kappa_p)] - \frac{4}{\pi^2} \left[\ln \left(\frac{|\kappa_p \mathcal{R}(\kappa - \kappa_p)|}{2} \right) + \gamma_E \right]^2 \right\} d\kappa, \quad (\text{A.32})$$

whose most divergent contribution is asymptotic to

$$\rho_{\text{R,L},p}^2 \sim \bar{\mathcal{E}} \epsilon [\ln(\kappa_p \mathcal{R} \epsilon)]^2 = \bar{\mathcal{E}} \epsilon \left[\ln \left(\frac{\kappa_p \epsilon}{\delta \kappa_p^2} \right) \right]^2. \quad (\text{A.33})$$

Notice again that the contribution to the SNR near the

pole is finite and in fact it formally vanishes in the limit $\delta \kappa_p \rightarrow 0$. As is clear from the above analysis, regularization is here justified: for a suitably small regularization interval ϵ , the contribution from a neighborhood ϵ around the pole is small. To provide a numerical example, saturating the Solar System constraint again ($\kappa_p = 150$ Hz) and choosing a regularization interval of size $\epsilon = 10^{-8}$ Hz we find that $\rho_{\text{R,L},p} \lesssim 30 \hat{\rho}_{\text{R,L},p}$, where $\hat{\rho}_{\text{R,L},p}$ is the contribution of the SNR in an interval of size $\delta \kappa_p$ in the absence of a resonance. The SNR is mostly dominated by contributions between 100-300 Hz, so splitting this region into segments of size $\delta f_p = 10^{-8}$ Hz, one obtains approximately 10^{10} segments. Assuming each segments carries approximately the same power, one can estimate that $\hat{\rho}_{\text{R,L},p} \sim 10/10^{10} = \mathcal{O}(10^{-9})$. Therefore, the contribution from the resonance that we lose by regularizing is approximately $\rho_{\text{R,L},p} \lesssim 10^{-8}$ and can be neglected.

-
- [1] J. S. Bell and R. Jackiw, *Nuovo Cim.* **A60**, 47 (1969).
 - [2] S. L. Adler, *Physical Review* **177**, 2426 (1969).
 - [3] L. Alvarez-Gaume and E. Witten, *Nucl. Phys.* **B234**, 269 (1984).
 - [4] M. B. Green, J. H. Schwarz, and E. Witten, *Superstring Theory. Vol. 2: Loop Amplitudes, Anomalies and Phenomenology* (Cambridge University Press (Cambridge Monographs On Mathematical Physics), Cambridge, UK, 1987).
 - [5] S. H. S. Alexander and J. Gates, S. James, *JCAP* **0606**, 018 (2006), hep-th/0409014.
 - [6] A. Ashtekar, A. P. Balachandran, and S. Jo, *Int. J. Mod. Phys. A* **4**, 1493 (1989).
 - [7] V. Taveras and N. Yunes, *Phys. Rev.* **D78**, 064070 (2008), 0807.2652.
 - [8] G. Calcagni and S. Mercuri, *Phys. Rev.* **D79**, 084004 (2009), 0902.0957.
 - [9] S. Mercuri and V. Taveras, *Phys. Rev.* **D80**, 104007 (2009), 0903.4407.
 - [10] S. J. Gates, Jr., S. V. Ketov, and N. Yunes, *Phys. Rev.* **D80**, 065003 (2009), 0906.4978.
 - [11] S. Alexander and N. Yunes, *Phys. Rept.* **480**, 1 (2009), 0907.2562.
 - [12] R. Jackiw and S. Y. Pi, *Phys. Rev. D* **68**, 104012 (2003).
 - [13] S. Weinberg, *The quantum theory of fields, Vol. 2: Modern applications* (Univ. Pr., Cambridge, UK, 1996).
 - [14] J. Polchinski, *String theory. Vol. 2 Superstring theory and beyond* (Univ. Pr., Cambridge, UK, 1998).
 - [15] S. Weinberg, *Phys. Rev.* **D77**, 123541 (2008), 0804.4291.
 - [16] C. R. Contaldi, J. Magueijo, and L. Smolin, *Phys. Rev. Lett.* **101**, 141101 (2008), 0806.3082.
 - [17] A. Lue, L.-M. Wang, and M. Kamionkowski, *Phys. Rev. Lett.* **83**, 1506 (1999).
 - [18] S. Alexander, L. S. Finn, and N. Yunes, *Phys. Rev.* **D78**, 066005 (2008), 0712.2542.
 - [19] N. Yunes and L. S. Finn, *J. Phys. Conf. Ser.* **154**, 012041 (2009), 0811.0181.
 - [20] S. H.-S. Alexander, M. E. Peskin, and M. M. Sheikh-Jabbari, *Phys. Rev. Lett.* **96**, 081301 (2006).
 - [21] S. Alexander and J. Martin, *Phys. Rev. D* **71**, 063526 (2005).
 - [22] S. Saito, K. Ichiki, and A. Taruya, *JCAP* **0709**, 002 (2007).
 - [23] N. Seto and A. Taruya, *Phys. Rev. Lett.* **99**, 121101 (2007).
 - [24] M. Satoh, S. Kanno, and J. Soda, *Phys. Rev. D* **77**, 023526 (2008).
 - [25] P. Laguna, S. L. Larson, D. Spergel, and N. Yunes, *Astrophys. J. Letts.* **715**, L12 (2010), 0905.1908.
 - [26] N. Yunes and C. F. Sopuerta, *Phys. Rev.* **D77**, 064007 (2008), 0712.1028.
 - [27] S. Alexander and N. Yunes, *Phys. Rev.* **D77**, 124040 (2008), 0804.1797.
 - [28] C. F. Sopuerta and N. Yunes, *Phys. Rev.* **D80**, 064006 (2009), 0904.4501.
 - [29] N. Gehrels et al., *AIP Conf. Proc.* **727**, 637 (2004).
 - [30] J. E. Carson, *J. Phys. Conf. Ser.* **60**, 115 (2007).
 - [31] B. Abbott et al., *Rept. Prog. Phys.* **72**, 076901 (2009), 0711.3041.
 - [32] F. Acernese et al. (Virgo), *Class. Quant. Grav.* **24**, S381 (2007).
 - [33] N. Seto, *Phys. Rev. D* **75**, 024016 (2007).
 - [34] N. Dalal, D. E. Holz, S. A. Hughes, and B. Jain, *Phys. Rev. D* **74**, 063006 (2006).
 - [35] S. Nissanke, S. A. Hughes, D. E. Holz, N. Dalal, and J. L. Sievers (2009), 0904.1017.
 - [36] S. Alexander and N. Yunes, *Phys. Rev. Lett.* **99**, 241101 (2007).
 - [37] S. Alexander and N. Yunes, *Phys. Rev.* **D75**, 124022 (2007).
 - [38] T. L. Smith, A. L. Erickcek, R. R. Caldwell, and M. Kamionkowski, *Phys. Rev. D* **77**, 024015 (2008).
 - [39] N. Yunes and D. N. Spergel, *Phys. Rev.* **D80**, 042004 (2009), 0810.5541.
 - [40] C. W. Misner, K. S. Thorne, and J. A. Wheeler (1979), *san Francisco* 1973, 1279p.
 - [41] S. Gukov, S. Kachru, X. Liu, and L. McAllister, *Phys. Rev. D* **69**, 086008 (2004).
 - [42] J. Abadie et al. (2010), 1003.2480.
 - [43] LIGO Scientific Collaboration, Tech. Rep., LIGO-T0900288-v3 (2009), URL <https://dcc.ligo.org/cgi-bin/DocDB/ShowDocument?docid=2974>.

- [44] G. M. Harry and the LIGO Scientific Collaboration, *Classical and Quantum Gravity* **27**, 084006 (2010).
- [45] N. Yunes and F. Pretorius, *Phys. Rev. D* **80**, 122003 (2009), 0909.3328.
- [46] C. Cutler and E. Flanagan, *Phys. Rev. D* **49**, 2658 (1994), gr-qc/9402014.
- [47] B. Abbott et al., *Phys. Rev. D* **77**, 062002 (2008), 0704.3368.
- [48] A. L. Stuver and L. S. Finn, *Class. Quant. Grav.* **23**, S799 (2006).
- [49] P. Grandclément, M. Ihm, V. Kalogera, and K. Belczynski, *Phys. Rev. D* **69**, 102002 (2004), arXiv:gr-qc/0312084.
- [50] A. M. Soderberg, E. Berger, M. Kasliwal, D. A. Frail, P. A. Price, B. P. Schmidt, S. R. Kulkarni, D. B. Fox, S. B. Cenko, A. Gal-Yam, et al., *Astrophys. J.* **650**, 261 (2006), astro-ph/0601455.
- [51] D. Grupe, D. N. Burrows, S. K. Patel, C. Kouveliotou, B. Zhang, P. Mészáros, R. A. M. Wijers, and N. Gehrels, *Astrophys. J.* **653**, 462 (2006), astro-ph/0603773.
- [52] C. Van Den Broeck and A. S. Sengupta, *Class. Quant. Grav.* **24**, 155 (2007), gr-qc/0607092.
- [53] N. Jarosik et al. (2010), 1001.4744.
- [54] K. Menou, Z. Haiman, and B. Kocsis, *New Astronomy Review* **51**, 884 (2008), 0803.3627.
- [55] A. Gal-Yam et al., *Astrophys. J.* **686**, 408 (2008), astro-ph/0509891.
- [56] E. Nakar, *Phys. Rept.* **442**, 166 (2007), arXiv:astro-ph/0701748.
- [57] N. Gehrels, J. K. Cannizzo, and J. P. Norris, *New Journal of Physics* **9**, 37 (2007).
- [58] M. Zemp, E. Ramirez-Ruiz, and J. Diemand, *Astrophys. J. Letters* **705**, L186 (2009), 0910.1593.
- [59] R. O’Shaughnessy, V. Kalogera, and C. Belczynski, *ApJ* **675**, 566+ (2008).
- [60] W. S. Paciesas, C. A. Meegan, G. N. Pendleton, M. S. Briggs, C. Kouveliotou, T. M. Koshut, J. P. Lestrade, M. L. McCollough, J. J. Brainerd, J. Hakkila, et al., *Astrophys. J. Suppl.* **122**, 465 (1999), arXiv:astro-ph/9903205.
- [61] D. Guetta and T. Piran, *Astron. Astrophys.* **435**, 421 (2005).
- [62] D. Guetta and T. Piran, *Astron. Astrophys.* **453**, 823 (2006).
- [63] B. Abbott et al., *Phys. Rev. D* **72**, 042002 (2005), gr-qc/0501068.
- [64] B. Abbott et al., *Phys. Rev. D* **77**, 062004 (2008), 0709.0766.
- [65] R. O’Shaughnessy, C. Kim, V. Kalogera, and K. Belczynski, *Astrophys. J.* **672**, 479 (2008).
- [66] R. O’Shaughnessy, V. Kalogera, and K. Belczynski, in preparation (2009).
- [67] C. M. Bender and S. A. Orszag, *Advanced mathematical methods for scientists and engineers 1, Asymptotic methods and perturbation theory* (Springer, New York, 1999).